Mechanisms of AAV neutralization by human alpha-defensins

Short Title: AAV neutralization by human alpha-defensins

Jessica M. Porter[a], Kaitlin R. Hulce[a], Mackenzi S. Oswald[a], Kevin Busuttil[b], Shanan N. Emmanuel[b], Antonette Bennett[b], Robert McKenna[b], and Jason G. Smith[a,#]

[a]Department of Microbiology, University of Washington School of Medicine, Seattle, Washington, USA

[b]Department of Biochemistry and Molecular Biology, University of Florida College of Medicine, Gainesville, Florida, USA

[#]Address correspondence to Jason G. Smith, jgsmith2@uw.edu

Abstract

Antiviral immunity compromises the efficacy of adeno-associated virus (AAV) vectors used for gene therapy. This is well understood for the adaptive immune response. However, innate immune effectors like alpha-defensin antimicrobial peptides also block AAV infection, although their mechanisms of action are unknown. To address this gap in knowledge, we investigated AAV2 and AAV6 neutralization by human neutrophil peptide 1 (HNP1), a myeloid alpha-defensin, and human defensin 5 (HD5), an enteric alpha-defensin. We found that both defensins bind to AAV2 and inhibit infection at low micromolar concentrations, similar to our prior studies of AAV6. While HD5 prevents AAV2 and AAV6 from binding to cells, HNP1 does not. However, AAV2 and AAV6 exposed to HD5 after binding to cells are still neutralized, indicating an additional block to infection. Accordingly, both HD5 and HNP1 inhibit externalization of the VP1 unique domain of both AAV2 and AAV6, which contains a phospholipase A_2 enzyme required for endosome escape and nuclear localization signals required for nuclear entry. Consequently, both defensins prevent AAV from reaching the nucleus. Disruption of intracellular trafficking of the viral genome to the nucleus is reminiscent of how alpha-defensins neutralize other non-enveloped viruses, suggesting a common mechanism of inhibition. These results will inform the development of vectors capable of overcoming these hurdles to improve the efficiency of gene therapy.

Author Summary

AAVs are commonly used as gene therapy vectors due to their broad tropism and lack of disease association; however, host innate immune factors, such as human alpha-defensin antimicrobial peptides, can hinder gene delivery. Although it is becoming increasingly evident that human alpha-defensins can block infection by a wide range of nonenveloped viruses, including AAVs, their mechanism of action remains poorly understood. In this study, we describe for the first time how two types of abundant human alpha-defensins neutralize two AAV serotypes, AAV2 and AAV6. We found that one defensin prevents AAV binding to cells, the first step in infection, while both defensins block a critical later step in AAV entry. Our findings support the emerging idea that defensins use a common strategy to block infection by DNA viruses that replicate in the nucleus. Through understanding how innate immune effectors interact with and impede AAV infection, vectors can be developed to bypass these interventions and allow more efficient gene delivery.

50 **Introduction**

51 Adeno-associated virus (AAV) is a non-enveloped single-stranded DNA virus that belongs
52 to the genus *Dependoparvovirus* of the *Parvoviridae* family. Their small icosahedral T=1 capsid
53 is comprised of three viral capsid proteins, VP1, VP2, and VP3, which assemble stochastically in
54 an approximately 1:1:10 ratio [1, 2]. There are currently 13 known AAV serotypes which were
55 isolated from both human and non-human primate species [3-5]. Due to their diverse tropism and
56 inability to replicate independently, recombinant AAVs (rAAVs) are used as gene therapy vectors
57 [6-8]. There are currently eight approved rAAV-based gene therapies, with more being tested in
58 clinical trials [8]. However, poor transduction efficiency and interactions with the host immune
59 system present hurdles that must be overcome to produce more efficient vectors [6, 7, 9, 10].
60 While the interactions of AAVs with components of the adaptive immune response such as anti-
61 capsid neutralizing antibodies [11-13] and T cells [14, 15] have been previously investigated, the
62 interactions of AAVs with innate immune effectors including antimicrobial peptides such as human
63 α-defensins are vastly understudied.

64 Defensins are short, amphipathic, and cationic innate immune peptides that have been
65 studied for their antimicrobial properties [16, 17]. They are broadly antimicrobial against bacteria
66 and fungi as well as enveloped and non-enveloped viruses. Their structures consist primarily of
67 β-sheets stabilized by three disulfide bonds [16, 18, 19]. Some defensins also form dimers, which
68 are essential for their antiviral activity [20-23]. There are two types of defensins produced by
69 humans, α- and β-defensins. Human α-defensins can be further categorized into two subtypes:
70 enteric and myeloid. Enteric α-defensins, human defensin 5 and 6 (HD5 and HD6), are
71 constitutively secreted by Paneth cells in the crypts of the small intestine at low mM concentrations
72 and are also present in the genitourinary tract [24-27]. Myeloid α-defensins, human neutrophil
73 peptides 1 to 4 (HNP1 to HNP4), are primarily expressed in neutrophils, where they are stored in
74 cytoplasmic azurophilic granules that fuse with phagolysosomes following uptake of bacteria and

75 viruses [16, 17, 19]. In addition, neutrophils release HNPs into the extracellular space during the
76 formation of neutrophil extracellular traps [28]. Although plasma or serum concentrations of HNPs
77 in healthy individuals are in the low nM range, they can be elevated in patients with liver disease,
78 bacterial meningitis, and some cancers, for which they have been investigated as biomarkers [29-
79 34]. Notably, plasma HNP1 concentrations as high as 49 μM have been measured in patients at
80 the onset of sepsis [34]. HNPs are also found in fluids lining epithelial surfaces including tears,
81 where HNP1 concentrations of 0.5 μM in normal tears are elevated 10-fold post-operatively or in
82 some diseased conditions [35, 36], and in the epithelial lining fluid of the lungs, where HNP1
83 concentrations of 31 to 79 nM in healthy patients are elevated up to 2.5 mM in diseased states
84 such as cystic fibrosis [37].

85 While both α- and β-defensins have been shown to have activity against bacteria and
86 enveloped viruses, only α-defensins inhibit non-enveloped viral infection [18, 19]. Human
87 adenovirus (HAdV), human papilloma virus (HPV), polyoma virus, and rotavirus (RV) have all
88 been shown to be sensitive to neutralization by either HD5, HNP1, or both [38-45]. Previously,
89 Virella-Lowell and colleagues found that AAV2 can be inhibited by HNPs present in
90 bronchoalveolar fluid and by a mixture of purified HNP1 and HNP2 [37]. We recently showed that
91 AAV1 and AAV6 are also neutralized by both HNP1 and HD5 [22]. In our previous studies with
92 HAdV and HPV, we found that α-defensins perturb viral uncoating, therefore preventing
93 productive infection [38, 40, 41, 46, 47]. A similar mechanism was determined for JC polyomavirus
94 neutralization by HD5 [44]. These findings suggest the possibility of a common mechanism
95 utilized by defensins to block non-enveloped viral infection. However, alternative mechanisms of
96 neutralization have also been described for polyomaviruses [43], and the molecular basis for
97 defensin-mediated inhibition of parvoviruses and rotaviruses has not been elucidated.

98 To begin to determine how α-defensins inhibit AAV, we focused on AAV2 and AAV6. We
99 found that like the previously described effects of myeloid α-defensins HNP1 and HNP2 [37], the

100 human enteric α-defensin HD5 also neutralizes AAV2. We then sought to determine the stage of
101 the AAV cell entry pathway that is perturbed by each defensin. Although HD5 but not HNP1 could
102 inhibit AAV2 and AAV6 from binding to cells, both defensins were able to neutralize AAV2 and
103 AAV6 when added post-attachment, suggesting a common block at a downstream step.
104 Consistent with this notion, we found that both defensins inhibit the externalization of the unique
105 domain of VP1 (VP1u), a crucial step in AAV entry. This in turn prevents endosome escape and
106 nuclear localization. Our findings support the concept of a common mechanism by which human
107 α-defensins neutralize non-enveloped viruses by perturbing intracellular trafficking but also reveal
108 a novel AAV-specific mechanism.

109 **Results**

110 **Both HD5 and HNP1 bind to AAV2 and neutralize infection**

111 Prior studies have shown that human enteric and myeloid α-defensins may differentially
112 impact infection of non-enveloped viruses, including AAV1 [22, 38, 42, 44, 48]. Accordingly, we
113 first sought to determine the effects of HD5 and HNP1 on AAV2 infection using the same
114 physiologic defensin concentrations from our previous study of AAV1 and AAV6 [22]. When
115 incubated with AAV2 on ice before the mixture is added to cells (pre-attachment), both HD5
116 [inhibitory concentration (IC_{50}), 7.5 μM; 95% confidence interval (CI), 6.8 to 8.3 μM; Hill slope, -4.0]
117 and HNP1 (IC_{50}, 9.7 μM; 95% CI, <10.7 μM; Hill slope, -19.8) inhibit AAV2 infection with similar
118 potency, and complete neutralization is achieved by 40 μM HD5 and 20 μM HNP1 (Fig 1A and
119 1B). We then quantified binding of each defensin to the AAV2 capsid by monitoring real-time
120 kinetics of their interaction using surface plasmon resonance (SPR). Consistent with our studies
121 of AAV1 and AAV6 [22], both defensins bind to the AAV2 capsid (Fig 1C and 1D). HNP1
122 [equilibrium dissociation constant (K_D) = 0.32 ± 0.03 μM] bound with approximately 1.8-fold
123 greater avidity than HD5 (K_D = 0.57 μM ± 0.06 μM), while the stoichiometry of HD5 (385 ± 5
124 molecules per capsid) was approximately 1.7-fold greater than HNP1 (227 ± 10 molecules per

125 capsid). Thus, in contrast to our prior findings with AAV1 and AAV6 where both defensins bind to
126 each serotype with similar avidity, HNP1 binds more tightly than HD5 to AAV2. However, as was
127 true for AAV1 and AAV6, more HD5 than HNP1 binds to AAV2.
128
129 **HD5, but not HNP1, inhibits AAV2 binding to cells**
130 To elucidate the mechanisms by which HD5 and HNP1 inhibit AAV2 infection, we first
131 determined if either defensin could block AAV2 from binding to cells. We used qPCR to enumerate
132 viral particles bound to cells in the cold in the presence or absence of increasing concentrations
133 of defensin. HD5 (IC_{50}, 9.2 μM; 95% CI, 6.7 to 14.1 μM; Hill slope, -3.7), but not HNP1, inhibited
134 AAV2 cell binding (Fig 2A and B). Moreover, the IC_{50} of HD5 for binding (Fig 2A) and infection
135 (Fig 1A) are equivalent ($P = 0.94$), suggesting that disrupted binding is the primary mechanism
136 HD5 employs to block infection. We therefore reasoned that binding the virus to cells prior to
137 defensin exposure might bypass inhibition of infection by HD5. However, contrary to our
138 expectations, HD5 still neutralized infection when added post-attachment (IC_{50}, 4.4 μM; 95% CI,
139 3.9 to 4.9 μM; Hill slope, -3.0) (Fig 2C). HNP1 also inhibited AAV2 under these conditions (IC_{50},
140 6.0 μM; 95% CI, 5.4 to 6.6 μM; Hill slope, -3.8), as expected (Fig 2D). Furthermore, as was true
141 for AAV6 [22], both HD5 and HNP1 were more potent inhibitors of infection when added post-
142 attachment rather than pre-attachment (HD5, $P < 0.0001$; HNP1, $P = 0.0008$). Thus, while
143 inhibition of cell binding likely contributes to AAV2 neutralization by HD5, both defensins mediate
144 a block of infection downstream of binding.
145
146 **HD5 and HNP1 inhibit exposure of VP1u**
147 A critical post-binding step in AAV entry is endosome escape mediated by the
148 phospholipase A_2 (PLA2) domain of VP1u. Before AAV enters the cell, VP1u is held within the
149 capsid. However, conformational changes to the capsid occur within the endosome, resulting in
150 externalization of VP1u [49-53]. To determine if this conformational change is disrupted by

151 defensin interactions, we utilized antibodies [54] that bind either the externalized VP1u subunit
152 (A1) or an epitope on the exterior of the VP3 domain (A20) in immunoprecipitation assays. HeLa
153 cells infected with AAV2 in the presence or absence of an inhibitory concentration of HD5 or
154 HNP1 were harvested 6 h post-infection (p.i.), and virus was precipitated from cleared lysate first
155 by the A1 antibody then by the A20 antibody. Precipitated virus was visualized by immunoblot
156 using the B1 antibody against VP1, VP2, and VP3 [54, 55]. Because VP3 is more abundant
157 (approximately 10 VP3 to 1 VP1) and A1 binding to VP1u precipitates the entire capsid with which
158 it is associated, we quantified the ratio of VP3 in the A1 blots to VP3 in the A20 blots across
159 replicates. In the absence of defensin, both A1 and A20 bound AAV2 (Fig 3A-H). However, either
160 25 μM HD5 (Fig 3A and 3B) or 30 μM HNP1 (Fig 3C and 3D) was sufficient to block A1 binding,
161 suggesting the absence of accessible VP1u. These defensin concentrations also completely
162 inhibited infection under the conditions of this assay (Fig 3I-K). To exclude the possibility that the
163 lack of A1 binding or accessibility was due to defensins competing with A1 for its epitope in VP1u,
164 we infected cells in the absence of defensin, harvested at 5 h p.i. (for HD5) or 6 h p.i. (for HNP1),
165 and then added HD5 or HNP1 to the cleared lysate during immunoprecipitation with A1 and A20.
166 Under these conditions, both antibodies reacted with AAV2 (Fig 3E-H), indicating that the
167 defensins are unable to compete with antibody binding. As an additional control, we utilized an
168 HD5 analog (HD5abu) that is incapable of forming disulfide bonds due to the substitution of α-
169 aminobutyric acid for the six cysteine residues in the linear sequence of HD5, rendering it non-
170 functional as an antiviral (Fig 3I and 3K) [22]. HD5abu had no effect on A1 binding (Fig 3A and
171 3B), supporting the conclusion that the lack of A1 reactivity in the presence of HD5 or HNP1 is
172 due to a specific effect of the defensins. From these experiments, we conclude that once the virus
173 is internalized, both HD5 and HNP1 can prevent externalization of the VP1u subunit.

174 To extend these findings to another serotype, we turned to AAV6, which is neutralized by
175 both HNP1 and HD5 when added either pre- or post-attachment (Fig 4A and 4B and [22]). As was
176 true for AAV2, HD5 but not HNP1 blocked AAV6 binding to cells (Fig 4A and 4B). However, while

177 the correlation between inhibition of binding and infection by HD5 for AAV2 was 1:1, ~4-fold more
178 HD5 was required to block AAV6 binding (IC_{50}, 41.6 μM; Hill slope, -0.9) than infection (IC_{50}, 10.0
179 μM [22]). Because inhibition of cell binding by HD5 was incomplete, we performed additional
180 control experiments with two known inhibitors of AAV6 binding and infection, the ADK1a
181 neutralizing antibody [56, 57] and wheat germ agglutinin [58]. Both controls effectively blocked
182 AAV6 binding, suggesting that the inability of HD5 to completely block AAV6 binding is not due to
183 a limitation of the assay (Fig 4C). We then examined the effects of HD5 and HNP1 on VP1u
184 exposure by AAV6. The A1 epitope is sufficiently conserved in AAV6; however, we used the
185 ADK1a antibody in place of A20 to precipitate intact AAV6 capsids. We also performed
186 immunoprecipitations 5 h p.i. and increased the scale of our experiments three-fold to maximize
187 the A1 signal. We found that both defensins prevented AAV6 VP1u exposure, however, inhibition
188 of both VP1u exposure (Fig 4D and 4F) and infection (Fig 4E and 4G) was less complete than we
189 observed for AAV2. Taken together, we conclude that this mechanism of neutralization is
190 conserved between at least two AAV serotypes.
191
192 **Thermostability of the AAV2 capsid is not altered by either defensin**
193 During these experiments, we noticed the appearance of a weak, virus-specific band in
194 the A20-precipitated AAV2 samples that was only present in the absence of defensin (arrows, Fig
195 5A and 5B). Although it was not always observable in controls, likely due to the limit of detection
196 of the assay, it was always absent or noticeably reduced in defensin-treated samples. The mobility
197 of this band was faster than VP3, suggesting that it may be a proteolytic degradation product of
198 one or more capsid proteins that retains the B1 epitope. We have previously described such
199 degradation products of AAV2 capsids [59, 60]. The absence of this band in samples treated with
200 either HD5 or HNP1 suggested that the defensins may be stabilizing the capsid and preventing
201 proteolysis. Note that for AAV6, this region of the immunoblot is masked by strong signal from the
202 ADK1a antibody heavy chain, making it difficult to assess if the same degradation product is

203 present for this serotype. Thus, we focused follow-up studies on AAV2 to assess whether
204 defensins alter capsid stability. To measure AAV2 capsid stability more broadly, we utilized
205 differential scanning fluorimetry (DSF) in the presence or absence of either 25 μM HD5 or 30 μM
206 HNP1 over a pH range from 4.0 to 7.4. This method uses the fluorescence of SYPRO Orange
207 dye as a function of temperature to determine the melting temperature (T_m) of the capsid. Although
208 we observed a stabilizing effect of pH, with a maximal T_m of 78.2°C at pH 5.5 compared to 66.4°C
209 at pH 7.4 and 74.2°C at pH 4.0, as observed previously [61], there was no effect of either defensin
210 on thermostability (Fig 5C). These results suggest that defensin binding to the capsid might block
211 specific conformational changes required for VP1u externalization or access of proteases to
212 cleavage sites rather than creating an overall more stable capsid.

213

214 **AAV2 fails to enter the nucleus and accumulates perinuclearly in the presence of defensins**

215 VP1u externalization serves at least two functions in AAV entry. The VP1u PLA2 domain
216 disrupts the endosomal membrane, and VP1u contains nuclear localization signals that facilitate
217 entry of the cytoplasmic capsid into the nucleus [50, 52, 62]. Therefore, we hypothesized that an
218 inability of AAV2 to externalize VP1u in the presence of defensins would manifest as a reduction
219 in nuclear localization of the capsid. We used confocal microscopy to visualize the trafficking of
220 DyLight 488 (DL488)-labelled AAV2 in the presence and absence of a neutralizing concentration
221 of either HD5 or HNP1. For these experiments, HD5 and HNP1 were added post-attachment due
222 to the reduction in cell binding by HD5 when added to AAV2 pre-attachment. In the absence of
223 defensin at 0 h p.i., DL488 AAV2 signal is diffuse with only coincidental colocalization with the
224 nuclear marker (DAPI) in z-projected images (Fig 6A-C), consistent with the virus being bound to
225 the outside of the cell. In contrast, at 24 h p.i., the viral signal is more punctate, and pronounced
226 nuclear localization is observed. In the presence of either HD5 or HNP1 at inhibitory
227 concentrations, AAV2 is punctate but exhibits markedly reduced nuclear localization. Rather, the

228 virus accumulates perinuclearly, which we quantified by measuring the fraction of viral signal in
229 each cell in a region spanning 5 pixels into and 50 pixels outside of the nucleus (Fig 6D). In
230 untreated samples, the perinuclear fraction is smaller than the nuclear fraction; however, the ratio
231 is reversed in HD5- or HNP1-treated samples (Fig 6E). Moreover, the absolute intensity of AAV2
232 at 24 h p.i. in defensin-treated samples is higher than in untreated samples (Fig 6F), which is
233 consistent with reduced proteolytic degradation (Fig 5A and 5B). These data, in combination with
234 the lack of A1 reactivity described above, support a model whereby both HD5 and HNP1 block
235 VP1u externalization during entry, thereby impeding AAV2 from reaching the nucleus and
236 neutralizing infection.
237
238 **Discussion:**

239 In this study, we have demonstrated that AAV2 infection is neutralized by both enteric and
240 myeloid α-defensins with similar potency, extending our previous studies of AAV1 and AAV6 to
241 an additional serotype [22]. In a normal infection, AAV binds to cells through interactions with
242 attachment factors (e.g., heparan sulfate proteoglycans for AAV2 and proteoglycans with heparan
243 sulfate or terminal sialic acids for AAV6) [63-65] and is endocytosed (Fig 7, left). In the endosome,
244 the VP1u subunit, which was kept within the capsid prior to entry, is externalized [8, 49-52, 66].
245 This step is crucial for AAV entry, as the VP1u PLA2 domain mediates breakdown of the
246 endosomal membrane, allowing virions to escape into the cytosol [53]. Host factors required for
247 these steps are incompletely understood, but changes in pH and interactions with recently
248 identified proteinaceous host factors including KIAA0319L (AAVR) and GPR108 play important
249 roles [8, 66-70]. Once released from the endosome, AAV traffics along microtubules, and nuclear
250 localization signals in VP1 and VP2 mediate entry of the virion into the nucleus [52, 62, 71-73].
251 The virion then uncoats in the nucleolus, releasing its genome to begin transcription and
252 replication [74, 75]. In the presence of defensins, two crucial steps in this entry pathway are

253 perturbed: cell binding and VP1u exposure (Fig 7, right). HD5 but not HNP1 perturbs cell binding,
254 if encountered by AAV2 or AAV6 prior to cell attachment. However, if AAV2 or AAV6 succeeds in
255 binding to the cell and becomes internalized, HD5 and HNP1 both prevent the externalization of
256 the VP1u subunit downstream of cell binding, thereby trapping the virus in the endosome and
257 blocking cellular trafficking and nuclear entry.

258 How defensins interact with the capsid to block VP1u externalization remains unknown. A
259 reasonable expectation is that both defensins must remain bound to the capsid at endosomal
260 pHs, which are required to stimulate conformational changes required for VP1u externalization in
261 the absence of defensin. However, it is possible that as the pH environment of the capsid changes
262 during endocytosis, defensin binding is altered but not completely abrogated. There are at least
263 two models by which defensin binding may prevent VP1u externalization: 1) altering the local
264 chemical environment of pH-sensitive residues that form a “molecular switch” to trigger VP1u
265 externalization [59], thereby impeding their protonation or 2) blocking the conformational changes
266 that allow VP1u to be externalized through local stabilization or steric hinderance. These
267 mechanisms are not mutually exclusive. One model is that VP1u is externalized through channels
268 at the 5-fold axes that are too small to accommodate folded VP1u prior to conformational changes
269 induced by the endosomal environment [76, 77]. In addition to localized changes at the 5-fold
270 vertices, more extensive rearrangements involving other areas of the capsid including the 2-fold
271 axis have been postulated [76, 78]. Our data suggest that defensins do not increase the overall
272 thermostability of the AAV2 capsid, arguing against a model where the entire capsid is stabilized
273 against host-induced conformational changes upon defensin binding. However, steric hinderance
274 at the 5-fold axis pore may prevent either the necessary local conformational changes from
275 occurring or block VP1u from threading through the pore. A similar model has been postulated
276 for the anti-AAV8 and -AAV9 antibody HL2372 and the POROS CaptureSelect affinity ligand
277 CSAL9, both of which bind to the 5-fold axis and neutralize infection [79-81]. In our prior studies

278 of differences in defensin sensitivity of AAV1 and AAV6, the crucial residue was located at position
279 531 located on the arm of the 3-fold protrusion extending along the wall of the 2-fold axis [22]. A
280 positively charged residue at this location (lysine) was associated with more uniform sensitivity to
281 defensin neutralization. In contrast, viruses bearing a negatively charged residue (glutamic acid)
282 had variable phenotypes dependent upon when defensin was added relative to cell binding.
283 Therefore, we hypothesized that amino acid 531 is not directly involved in binding to cationic
284 defensins. Rather, the nature of this residue may dictate surface charge at other parts of the
285 capsid to modulate defensin interactions. Definitive mechanistic insight awaits structural
286 information on the defensin-AAV complexes.

287 An additional hint to the location of defensin interactions with AAV may be obtained by
288 further analysis of capsid protein proteolysis that appears to be blocked by both HD5 and HNP1
289 binding. Studies of purified virus have shown that AAVs possess intrinsic autoproteolytic activity
290 that is activated at endolysosomal pH leading to degradation of VP1 and VP3 (and possibly VP2)
291 [59] in addition to protease activity in the VP1u domain that is capable of cleaving external
292 substrates (e.g., casein) [59, 82]. Thus, the absence of capsid degradation in the presence of α-
293 defensins could constitute additional evidence that VP1u is not externalized and able to cleave
294 the capsid. Alternatively, it could reflect direct inhibition of auto-proteolytic activity elsewhere in
295 the capsid or capsid cleavage by cellular proteases during infection. In this regard, HD5 and HNP1
296 could block either the protease active site or the target cleavage site. To our knowledge, there
297 have been no studies of inhibitors or mutants that have elucidated the role of capsid cleavage in
298 AAV infection, although cleavage of the capsid proteins of autonomous parvoviruses by
299 autoproteolysis or cellular proteases is an important step in maturation or entry [83-85]. Thus,
300 further study of the inhibition of capsid cleavage may provide insight into where defensins bind to
301 the capsid, but it is unclear if blocking proteolysis contributes to the defensin-mediated
302 neutralization mechanism.

303 Although both HD5 and HNP1 block VP1u externalization, their interactions with the
304 capsid differ. First, only HD5 disrupts AAV2, and less potently AAV6, from binding to cells. This
305 mode of neutralization by α-defensins is uncommon, having only been described previously for
306 BK polyomavirus, where HD5 aggregates the virus and reduces cell binding [43]. In contrast, cell
307 binding of many viruses like HAdVs, mouse AdV, and HIV-1 is promoted by α-defensins [39, 46,
308 86-88]. Second, HNP1 binds AAV2 more tightly than HD5 does, but there is less HNP1 than HD5
309 bound to the capsid at equilibrium. These differences are not surprising given that the two
310 defensins, although structurally similar, vary in primary sequence, net charge, and charge
311 distribution. Unlike antibodies, defensins do not bind to a specific epitope. Rather, selective
312 binding to favorable capsid regions may initially occur over a range of affinities. Primary binding
313 may then promote additional defensin-defensin and defensin-capsid interactions. HD5, with
314 weaker but more abundant binding, may sterically occlude heparan sulfate proteoglycan (HSPG)
315 binding sites, inhibiting cell binding. HNP1 instead may bind preferentially to less abundant, higher
316 affinity sites away from the HSPG binding site, allowing cell binding to occur. The importance of
317 stoichiometry in blocking receptor binding is underscored by the phenotype of AAV6, where both
318 defensins bind with similar affinity [22]. However, HD5 is not only more abundant on the capsid
319 but also capable of blocking cell binding despite the ability of AAV6 to utilize either HSPG or
320 terminal sialic acid for attachment. Thus, it is reasonable to postulate that the binding sites utilized
321 by each defensin may not entirely overlap. These findings are reminiscent of HPV interactions
322 with defensins, where genital types differ in their sensitivities to HD5 and HNP1 and where HD5
323 inhibits multiple steps of HPV16 entry [40-42].

324 By blocking the externalization of VP1u, the PLA_2 domain is unable to access the limiting
325 membrane, likely trapping the virus within the endosome. This interpretation is based on the
326 failure of defensin-treated virus to reach the nucleus; however, we did not measure endosomal
327 escape directly. It is plausible that defensins bound to the capsid could mediate endosome escape

328 through their ability to form pores in lipid bilayers [89]. In this case the absence of externalized
329 nuclear localization signals found in VP1u and the VP1/2 common region would still prevent the
330 virus from reaching and entering the nucleus [52, 62]. Thus, the increased amount of detectable
331 virus in defensin-treated samples at 24 h p.i. could be explained by defensin-induced viral
332 aggregation in either the endosome or cytoplasm, protection of virus trapped in the
333 endolysosomal system from lysosomal degradation, or protection of virus in the cytoplasm from
334 ubiquitination and proteosomal degradation. These mechanisms are not mutually exclusive,
335 although we note that all samples are treated with the proteosome inhibitor doxorubicin, which
336 has been shown to increase AAV transduction efficiency [90].

337 Without additional experimentation, it is difficult to anticipate the generalizability of our
338 findings to other AAV serotypes. Both AAV2 and AAV6 are neutralized by both HD5 and HNP1
339 when added to the virus either pre- or post-attachment to the cell [22]. However, the sensitivity of
340 AAV1 to each defensin depends on the order-of-addition, where HD5 is only neutralizing when
341 added pre-attachment and HNP1 is only neutralizing when added post-attachment. As described
342 above, the identity of residue 531 in VP3 solely dictates the defensin sensitivities of AAV1 and
343 AAV6. Although the defensin-dependent phenotypes of AAV2 and AAV6 are more similar, AAV2
344 and AAV1 (not AAV6) have the same residue (glutamic acid) at this position. Thus, the identity of
345 the residue at position 531 is not predictive. AAV2 and AAV6 share the ability to utilize HSPG as
346 an attachment factor [64], while AAV1 uses sialic acid [65]. Therefore, the nature of the
347 attachment factor might correlate with defensin sensitivity, particularly regarding blocking cell
348 binding. Until more serotypes are studied and a completely defensin-resistant serotype is
349 identified, it is hard to determine which characteristics might foretell defensin sensitivity; however,
350 our findings provide a blueprint for key assays that will inform neutralization mechanisms.

351 Finally, our findings may inform the development of AAV vectors. HNP levels are
352 increased in patients with highly inflammatory disease states, such as cystic fibrosis, which would

353 impair the delivery of gene therapy by defensin-sensitive serotypes such as AAV2 [37]. By
354 identifying where in the entry pathway innate immune peptides such as defensins inhibit, mutant
355 vectors can be better designed with the goal of escaping neutralization. Alternatively, existing
356 vectors that have been customized for tropism or antibody escape can be further tested for
357 defensin sensitivity [8]. Importantly, our findings provide two points of likely inhibition, cell binding
358 and endosome escape, that can be targeted in the development of escape variants.

359 **Materials and Methods**

360 **Cells.** HeLa (ATCC) and HEK293 cells (ATCC or University of Florida Powell Gene Therapy
361 Center Vector Core) were cultured in Dulbecco's modified Eagle's media (DMEM) supplemented
362 with 10% Fetal Bovine Serum (FBS), 0.1 mM non-essential amino acids, 4 mM L-glutamine, 100
363 units/mL penicillin, and 100 µg/mL streptomycin.

364 **Vector production and purification.**

365 AAV2 and AAV6 vectors expressing GFP were produced by triple transfection in mammalian
366 HEK293 cells. HEK293 cells were cultured to approximately 80% confluency in 150 mm cell
367 culture dishes and triple transfected with an equimolar ratio of pXRAAV2 [91], pTR-UF11-GFP
368 [92], and pXX6 (pHelper) [93] plasmids (totaling 40 µg/plate), which were diluted with 1 mL
369 Optimem (Gibco) and 125 µL of 1 mg/ml polyethyleneimine (PEI) per plate. For AAV6, pXR6 [64]
370 was substituted for pXRAAV2. The solution was incubated for 15 min at RT and added dropwise
371 to each plate. Cells were harvested 72 h post-transfection and separated from the supernatant
372 by centrifugation at 1100 × g in a JA-20 rotor at 4°C for 15 min. The cell pellet was resuspended
373 in 1 mL/plate of TD buffer (1X PBS, 5 mM $MgCl_2$, 2.5 mM KCl, pH 7.4) and lysed by three
374 freeze/thaw cycles, followed by Benzonase (Promega) treatment at 37°C for 1 h. The cellular
375 debris was removed by centrifugation at 3000 × g, and the clarified cell lysate was stored at -80°C.
376 The supernatant was PEG precipitated overnight with 10% (w/v) PEG 8000 (Fisher) and then
377 centrifuged at 14,300 × g in a JA-10 rotor at 4°C for 90 min. The resulting PEG pellet was
378 resuspended in 1 mL/plate of TD buffer and clarified by centrifugation at 3000 × g. The
379 supernatant was then combined with the cell lysate, and AAV capsids were purified by AVB affinity
380 chromatography on a 1 mL AVB Sepharose affinity chromatography column (Cytvia,
381 Marlborough, MA), as previously described [64, 94]. Virus was eluted with 10 mL of elution buffer
382 (0.1 M glycine-HCl, pH 2.7) and neutralized with 1 mL of neutralization buffer (1 M Tris-HCl, pH

383 10.0). The final sample was concentrated and buffer exchanged using an Apollo concentrator
384 (Orbital Bioscience), and the purity was verified by SDS-PAGE.

385 For confocal microscopy, purified AAV2 at approximately 0.5 mg/mL was extensively dialyzed
386 into PBS and labeled with the DyLight 488 Antibody Labeling Kit (Thermo Fischer) according to
387 the manufacturer's protocol. The completed reaction was dialyzed three times into PBS. Labeled
388 virus was visualized by SDS-PAGE using UV light to detect the fluorophore and quantified by
389 Coomassie Blue staining against BSA standards.

390 **α-defensin peptides.** HD5 (ATCYCRTHECATRESLSGVCEISGRLYRLCCR) and HNP1
391 (ACYCRIPACIAGERRYGTCIYQGRLWAFCC) were synthesized by CPC Scientific (Sunnyvale,
392 CA) and processed as previously described [45]. In brief, peptides were folded and stabilized by
393 thiol-disulfide reshuffling and purified by reverse-phase high-pressure liquid chromatography (RP-
394 HPLC) to homogeneity. Purity was analyzed by analytical RP-HPLC, verified by mass
395 spectrometry, and quantified by UV absorbance at 280 nm. HD5abu synthesis, purification, and
396 validation have been described previously [20, 21].

397 **Primary antibodies.** A1 (American Research Products, 03-61056) binds an epitope in VP1u [54,
398 55]. A20 (American Research Products, 03-61055) binds an epitope in the VP1/VP2/VP3
399 common domain of intact AAV2 [55]. ADK1a (University of Florida Hybridoma Core) binds an
400 epitope in the VP1/VP2/VP3 common domain of intact AAV1 and AAV6 [57, 95]. B1 (University
401 of Florida Hybridoma Core) binds an epitope in the VP1/VP2/VP3 common domain of uncoated
402 AAV2 and AAV6 [54, 55].

403 **Infection assays.** Infection assays were performed as previously described [22]. All viruses and
404 defensins were diluted in serum-free DMEM (SFM) supplemented with 1 μM doxorubicin (Dox).
405 AAV2 was diluted to 5.4E+10 viral genomes (vg)/mL for pre-attachment and 1.4E+11 vg/mL for
406 post-attachment. In brief, for pre-attachment exposure of AAV2 to defensins, 28 μL of AAV2 and
407 28 μL of SFM with or without HD5 or HNP1 were mixed and incubated on ice for 45 min before

408 50 µL of the mixture was added to cells. Samples were then incubated at 37°C. For post-
409 attachment exposure of AAV2 to defensins, 50 µL AAV2 was added to chilled cells and allowed
410 to bind for 1 h at 4°C. Samples were washed twice with ice-cold SFM before 50 µL SFM with or
411 without HD5 or HNP1 was added. Defensins were bound at 4°C for 45 min before cells were
412 moved to 37°C. For both conditions, 10 µL 60% FBS in SFM + 1 µM Dox was added to the wells
413 6 h p.i., but no additional washes were performed. At 48 h p.i., cells were washed with phosphate-
414 buffered saline (PBS), and total monolayer GFP fluorescence was quantified with an Azure
415 Sapphire. Background-subtracted total monolayer fluorescence was further analyzed with Fiji
416 (version 2.14.0/1.54f). Data are shown as the percentage of control infection in the absence of
417 defensin.

418 **SPR:** SPR experiments were performed on a BIAcore X100 instrument at 25°C, with PBS as the
419 running buffer, as previously described [22]. AAV2 was coupled to the CM5 sensor chip using
420 amine coupling, and 9451 response units (RUs) were immobilized. HD5 or HNP1 was the analyte,
421 and the same sensor chip was used for 2 replicate analyses on different days. Data were analyzed
422 as described previously to determine K_D, using the 1:1 binding model in BIAcore X100 evaluation
423 software (version 2.0.0), and stoichiometry, using GraphPad Prism (version 10.3.0).

424 **Cell binding assays:** HeLa cells were detached using 0.5 M EDTA, washed twice with cold SFM,
425 and resuspended in SFM + 0.2% sodium azide (SA). 8.4E+9 particles of AAV2 or AAV6 were
426 incubated with SFM + 0.2% SA with or without twice the final concentration of HD5, HNP1, or
427 ADK1a in a volume of 56 µL. Following incubation for 45 min on ice, 50 µL of the virus/defensin
428 mixture was added to 5.0E+5 HeLa cells in a final volume of 100 µL. For studies with wheat germ
429 agglutinin (WGA), cells were incubated with 50 µg/mL WGA for 10 min on ice, washed, and then
430 incubated with virus plus 50 µg/mL WGA. Samples were incubated for 90 min on ice with
431 intermittent agitation to allow binding. One sample without defensin was reserved as an input
432 control for quantitation. Remaining samples were washed three times with ice cold DMEM. All

433 samples were lysed and processed to extract genomic DNA using the Genejet Genomic DNA
434 Purification kit (Thermofisher) per the manufacturer's instructions. DNA was eluted from the
435 column in 100 µL elution buffer. qPCR was performed using SsoAdvanced SYBR Green master
436 mix (Bio-Rad) with primers for GFP (F: 5'-CCCAGACCATATGAAGCAGC-3'; R: 5'-
437 GCCCTTAGCTCGATTCTCT-3'). The absolute number of genomes bound to cells in each
438 condition was determined relative to a standard curve produced by a dilution series of the input
439 control. Note that diluting experimental samples 10-fold prior to analysis was required for accurate
440 quantitation. The amount of virus bound to cells in each condition within each replicate was then
441 normalized to the amount of virus bound to control cells in the absence of defensin.

442 **Immunoprecipitation and western blot:** HeLa cells were seeded at 6.0E+5 cells/mL in 6-well
443 plates and cultured overnight. Cells were infected with AAV2 or AAV6 at an MOI of 65,000 vg/cell
444 in 1 mL cold SFM. For AAV2, one well of cells was infected for each condition (ND, HD5, HNP1);
445 for AAV6, three wells were infected for each condition. After incubation for 1 h at 4°C while
446 rocking, the inoculum was removed and replaced with 1 mL SFM with or without 25 µM HD5, 25
447 µM HD5abu, or 30 µM HNP1. After an additional incubation for 45 min at 4°C while rocking, plates
448 were shifted to 37°C for 5 h (AAV6) or 6 h (AAV2). Cells were washed two times with ice cold
449 PBS, scaped to detach them from the plate, and concentrated in chilled 1.5 mL Eppendorf tubes
450 by centrifugation at 400 × g for 5 min at 4°C. The pellet was lysed in 100 µL immunoprecipitation
451 (IP) buffer (20 mM Tris, 137 mM NaCl, 1% Triton X-100, 2 mM EDTA, 1X HALT protease inhibitor,
452 pH 8), freeze-thawed three times, and centrifuged at 25,000 × g for 10 min at 4°C. Anti-AAV VP1
453 (A1, 200 ng) was added to the clarified lysate, and samples were incubated overnight at 4°C with
454 constant agitation. For control samples where defensin was added post-lysis, either HD5 (25 µM)
455 or HNP1 (30 µM) was added with A1. A1-bound AAV2 or AAV6 was precipitated with Protein G-
456 PLUS agarose beads (Santa Cruz Biotech). Anti-AAV2 VP1/2/3 (A20, 200 ng) or anti-AAV6
457 VP1/2/3 (ADK1a, 300 ng) was then added to the supernatant. Samples were incubated for ≥ 2 h

458 at 4°C with constant agitation and precipitated with Protein G-PLUS agarose beads. For both
459 precipitations, beads were washed three times with IP buffer, and samples were eluted with SDS-
460 loading buffer (3.2% SDS, 100 mM Tris, 0.04% bromophenol blue, 16% glycerol (w/v), 40 mM
461 dithiothreitol, pH 6.8). Heat-denatured (95°C for 5 min) samples were analyzed via SDS-PAGE
462 on 7.5% or 10% polyacrylamide gels, transferred to 0.45 µm nitrocellulose membranes, blocked
463 for 1 h at RT in blocking buffer [3% bovine serum albumin (BSA) and 1% Tween-20 in Tris-
464 buffered saline (TBS): 20 mM Tris, 150 mM NaCl, pH 8.0]. Membranes were incubated with anti-
465 AAV B1 antibody (333 ng/mL) in blocking buffer at 4°C overnight, washed three times in TBS +
466 1% Tween-20, probed with goat anti-mouse Alexa Fluor 488-conjugated secondary antibody
467 (ThermoFisher, A-11001, 1:1000) in blocking buffer, washed twice with TBS + 1% Tween-20 and
468 once with TBS, and imaged on an Azure Sapphire imager. Bands were quantified using
469 AzureSpot Pro (v2.1.097). For AAV2, data is the ratio of the background subtracted volume of the
470 A1 immunoprecipitated VP3 band divided by the A20 immunoprecipitated VP3 band for each
471 sample. For AAV6, the analogous A1/ADK1a ratio was normalized to the value for the no defensin
472 control.

473 **Differential Scanning Fluorimetry:** The stability of AAV2 was determined by differential
474 scanning fluorimetry (DSF) analysis using a Bio-Rad MyiQ2 Thermocycler to monitor the
475 fluorescence produced by the binding of SYPRO Orange dye (Invitrogen) to hydrophobic regions
476 of the AAV2 capsid upon heat denaturation. The temperature of the assay ranged from 30°C to
477 99°C, ramping at 0.5°C per step. Purified AAV2 (1 µg) was diluted in 22.5 µL of either 25 µM
478 HD5 or 30 µM HNP1 in citrate-phosphate (0.1 M citric acid, 0.2 M Na_2HPO_4) buffers at pH 7.4,
479 pH 6, pH 5.5, or pH 4. Samples were incubated for 30 min at RT before 2.5 µl/sample of 1%
480 SYPRO Orange dye was added. Samples containing buffer alone were used as negative
481 controls. Data is the inverse of the negative rate of change of relative fluorescence units vs

482 temperature (−dRFU/dT). The peak value on the resulting thermogram is the T_m. All experiments
483 were conducted in triplicate.

484 **Quantification of subcellular localization:** HeLa cells were cultured on glass coverslips
485 overnight. DyLight 488-labelled AAV2 in cold SFM containing 1 μM Dox at an MOI of 20,000
486 vg/cell was added, and cells were incubated for 1 h in the dark at 4°C. The inoculum was removed
487 and replaced with 50 μL SFM containing 1 μM Dox with or without 25 μM HD5 or 30 μM HNP1.
488 After incubation for 45 min at 4°C, one set of control coverslips was washed with PBS before
489 being fixed in 2% PFA (Electron Microscopy Science, 15710) for 15 min at RT. The remaining
490 cells were shifted to 37°C. At 6 h p.i., coverslips were moved to normal growth media, cultured
491 for an additional 18 h, washed with PBS, and fixed. Fixed cells were washed once with PBS and
492 incubated for 20 min at RT in permeabilization buffer (20 mM glycine, 0.5% Triton X-100, PBS).
493 Cells were sequentially stained with AF647-conjugated phalloidin (Abcam, ab176759, 1:1000) in
494 1% BSA, 0.05% Tween-80 in PBS for 45 min at RT then with 500 ng/mL DAPI for 5 min.
495 Coverslips were mounted with Prolong Gold (Life Technologies, P36930).

496 Z-series of images spanning entire cells were obtained using a confocal laser-scanning
497 microscope (Zeiss LSM 800) using a 63× objective. A maximum intensity z-projection of each
498 color channel for each field of view was generated using Fiji (v2.14.0/1.54h). Background
499 thresholds for AAV2 signal were determined manually for each replicate in Fiji using uninfected
500 negative controls. A human-in-the-loop model was trained in CellPose 2.0 [96] to identify cell
501 borders and generate cell masks. CellPose masks and z-projection images were imported into
502 CellProfiler (v4.2.5) [97], and background-subtracted single-cell images were identified and
503 exported. A second CellProfiler pipeline was then used to analyze the single-cell images. Nuclei
504 were identified using DAPI by thresholding using the Otsu method. A tertiary object extending 5
505 pixels into and 50 pixels beyond the nucleus was then defined as the perinuclear space, and the
506 integrated intensities of DyLight 488 within the whole cell, in the perinuclear space, and in the

507 nucleus were measured for each cell. Whole cells with DyLight 488 intensity < 100 relative
508 fluorescence units (RFU) were excluded from analysis.

509 **Statistical analysis:** All statistical analysis was performed with GraphPad Prism 10.3.0. Fig 1A,
510 1B, 2A, 2C, 2D, and 4A were analyzed by nonlinear regression using the "log (inhibitor) versus
511 response – variable slope (four parameters)" model with the bottom constrained to "0". Hill slopes
512 and IC_{50} values are the best-fit values. Log IC_{50} values were compared between protocol
513 conditions and assays (e.g., cell binding and inhibition of infection) using the extra-sum-of-
514 squares F test, and the P values are given. Fig 2B and 4B were analyzed by nonlinear regression
515 using the "log (agonist) versus response – variable slope (four parameters)" model without
516 constraint. Note that the AAV6 infection data in Fig 4A and 4B is reproduced from our prior study
517 for comparison [22]. In Fig 3B, 3K, 4C, 4F, and 4G, repeated measures one-way ANOVA using
518 Dunnett's multiple comparisons test with a single pooled variance was used to compare the mean
519 of each column with that of the "no defensin" control. In Fig 3D, 3F, and 3H a two-tailed, paired t
520 test was used to compare HD5 or HNP1 samples with "no defensin" controls. In Fig 3K, HD5 and
521 HD5abu were analyzed in parallel, while HNP1 was analyzed in separate experiments with
522 distinct "no defensin" controls. HD5, HD5abu, and HNP1 samples are graphed together for clarity.
523 Fig 5C was analyzed by repeated measures two-way ANOVA using Dunnett's multiple
524 comparisons test with a single pooled variance to compare the mean of each column with that of
525 the "no defensin" control for each pH value. Fig 6A, 6B, 6E and 6F were analyzed by ordinary
526 one-way ANOVA using Dunnett's multiple comparisons test with a single pooled variance to
527 compare the mean of each column with that of the "no defensin" control. In Fig 6A, each replicate
528 was analyzed individually. In Fig 6B, 6E, and 6F, the data for each condition for all replicates was
529 pooled prior to analysis. In Fig 6E and 6F, data was log-transformed prior to analysis. For all
530 analyses by ANOVA, P values are adjusted to account for multiple comparisons.

531

532 **Acknowledgements**

533 The authors would like to dedicate this study to the memory of Dr. Agbandje-McKenna, who was
534 a pioneer in the field of AAV structural biology. We thank Qun Tang and Melike Caglayan for
535 technical assistance with SPR experiments. We thank Dr. Matthew Parsek for the generous use
536 of his microscope and Dr. Jeffrey Carey and Dr. Xuhui Zheng in the Parsek lab for technical
537 assistance with microscopy. This work was supported by R01 AI104920 (to J.G.S. and R.M.) and
538 F32 AI178920 (to K.R.H.), from the National Institute of Allergy and Infectious Diseases
539 (www.niaid.nih.gov) and by the Office of the Director, National Institutes of Health
540 (www.nih.gov/institutes-nih/nih-office-director) under Award Number S10 OD026741 (to J.G.S.).
541 Additional support to J.G.S. in the form of subsidized core services was provided by NIH grants
542 UL1 TR000423 from the National Center for Advancing Translational Sciences (ncats.nih.gov),
543 and P30 CA015704 from the National Cancer Institute (www.cancer.gov). The funders had no
544 role in study design, data collection and analysis, decision to publish, or preparation of the
545 manuscript.

546 **References:**

547 1. Meyer NL, Chapman MS. Adeno-associated virus (AAV) cell entry: structural insights.
548 Trends Microbiol. 2022;30(5):432-51. Epub 20211025. doi: 10.1016/j.tim.2021.09.005.
549 PubMed PMID: 34711462.

550 2. Worner TP, Bennett A, Habka S, Snijder J, Friese O, Powers T, et al. Adeno-associated
551 virus capsid assembly is divergent and stochastic. Nature communications.
552 2021;12(1):1642. Epub 20210312. doi: 10.1038/s41467-021-21935-5. PubMed PMID:
553 33712599; PubMed Central PMCID: PMCPMC7955066.

554 3. Gao G, Vandenberghe LH, Alvira MR, Lu Y, Calcedo R, Zhou X, et al. Clades of Adeno-
555 associated viruses are widely disseminated in human tissues. J Virol. 2004;78(12):6381-8.
556 Epub 2004/05/28. doi: 10.1128/JVI.78.12.6381-6388.2004. PubMed PMID: 15163731;
557 PubMed Central PMCID: PMCPMC416542.

558 4. Schmidt M, Grot E, Cervenka P, Wainer S, Buck C, Chiorini JA. Identification and
559 characterization of novel adeno-associated virus isolates in ATCC virus stocks. J Virol.
560 2006;80(10):5082-5. doi: 10.1128/JVI.80.10.5082-5085.2006. PubMed PMID: 16641301;
561 PubMed Central PMCID: PMCPMC1472088.

562 5. Bossis I, Chiorini JA. Cloning of an avian adeno-associated virus (AAAV) and generation of
563 recombinant AAAV particles. J Virol. 2003;77(12):6799-810. doi: 10.1128/jvi.77.12.6799-
564 6810.2003. PubMed PMID: 12768000; PubMed Central PMCID: PMCPMC156192.

565 6. Large EE, Silveria MA, Zane GM, Weerakoon O, Chapman MS. Adeno-Associated Virus
566 (AAV) Gene Delivery: Dissecting Molecular Interactions upon Cell Entry. Viruses.
567 2021;13(7). Epub 20210710. doi: 10.3390/v13071336. PubMed PMID: 34372542; PubMed
568 Central PMCID: PMCPMC8310307.

569 7. Pillay S, Carette JE. Host determinants of adeno-associated viral vector entry. Curr Opin
570 Virol. 2017;24:124-31. Epub 20170630. doi: 10.1016/j.coviro.2017.06.003. PubMed PMID:
571 28672171; PubMed Central PMCID: PMCPMC5549665.
572 8. Lopez-Gordo E, Chamberlain K, Riyad JM, Kohlbrenner E, Weber T. Natural Adeno-
573 Associated Virus Serotypes and Engineered Adeno-Associated Virus Capsid Variants:
574 Tropism Differences and Mechanistic Insights. Viruses. 2024;16(3). Epub 20240312. doi:
575 10.3390/v16030442. PubMed PMID: 38543807; PubMed Central PMCID:
576 PMCPMC10975205.
577 9. Muhuri M, Maeda Y, Ma H, Ram S, Fitzgerald KA, Tai PW, et al. Overcoming innate immune
578 barriers that impede AAV gene therapy vectors. J Clin Invest. 2021;131(1). doi:
579 10.1172/JCI143780. PubMed PMID: 33393506; PubMed Central PMCID:
580 PMCPMC7773343.
581 10. Rabinowitz J, Chan YK, Samulski RJ. Adeno-associated Virus (AAV) versus Immune
582 Response. Viruses. 2019;11(2). Epub 20190125. doi: 10.3390/v11020102. PubMed PMID:
583 30691064; PubMed Central PMCID: PMCPMC6409805.
584 11. Scallan CD, Jiang H, Liu T, Patarroyo-White S, Sommer JM, Zhou S, et al. Human
585 immunoglobulin inhibits liver transduction by AAV vectors at low AAV2 neutralizing titers in
586 SCID mice. Blood. 2006;107(5):1810-7. Epub 20051025. doi: 10.1182/blood-2005-08-3229.
587 PubMed PMID: 16249376.
588 12. Boutin S, Monteilhet V, Veron P, Leborgne C, Benveniste O, Montus MF, et al. Prevalence
589 of serum IgG and neutralizing factors against adeno-associated virus (AAV) types 1, 2, 5,
590 6, 8, and 9 in the healthy population: implications for gene therapy using AAV vectors. Hum
591 Gene Ther. 2010;21(6):704-12. doi: 10.1089/hum.2009.182. PubMed PMID: 20095819.
592 13. Zaiss AK, Cotter MJ, White LR, Clark SA, Wong NC, Holers VM, et al. Complement is an
593 essential component of the immune response to adeno-associated virus vectors. J Virol.

594 2008;82(6):2727-40. Epub 20080116. doi: 10.1128/JVI.01990-07. PubMed PMID:
595 18199646; PubMed Central PMCID: PMCPMC2259003.
596 14. Arjomandnejad M, Sylvia K, Blackwood M, Nixon T, Tang Q, Muhuri M, et al. Modulating
597 immune responses to AAV by expanded polyclonal T-regs and capsid specific chimeric
598 antigen receptor T-regulatory cells. Mol Ther Methods Clin Dev. 2021;23:490-506. Epub
599 20211028. doi: 10.1016/j.omtm.2021.10.010. PubMed PMID: 34853797; PubMed Central
600 PMCID: PMCPMC8605179.
601 15. Basner-Tschakarjan E, Mingozzi F. Cell-Mediated Immunity to AAV Vectors, Evolving
602 Concepts and Potential Solutions. Front Immunol. 2014;5:350. Epub 20140723. doi:
603 10.3389/fimmu.2014.00350. PubMed PMID: 25101090; PubMed Central PMCID:
604 PMCPMC4107954.
605 16. Lehrer RI, Lu W. alpha-Defensins in human innate immunity. Immunol Rev. 2012;245(1):84-
606 112. Epub 2011/12/16. doi: 10.1111/j.1600-065X.2011.01082.x. PubMed PMID: 22168415.
607 17. Selsted ME, Ouellette AJ. Mammalian defensins in the antimicrobial immune response. Nat
608 Immunol. 2005;6(6):551-7. Epub 2005/05/24. doi: 10.1038/ni1206. PubMed PMID:
609 15908936.
610 18. Wilson SS, Wiens ME, Smith JG. Antiviral mechanisms of human defensins. J Mol Biol.
611 2013;425(24):4965-80. Epub 20131002. doi: 10.1016/j.jmb.2013.09.038. PubMed PMID:
612 24095897; PubMed Central PMCID: PMCPMC3842434.
613 19. Holly MK, Diaz K, Smith JG. Defensins in Viral Infection and Pathogenesis. Annual review
614 of virology. 2017;4(1):369-91. Epub 20170717. doi: 10.1146/annurev-virology-101416-
615 041734. PubMed PMID: 28715972.
616 20. Rajabi M, Ericksen B, Wu X, de Leeuw E, Zhao L, Pazgier M, et al. Functional determinants
617 of human enteric alpha-defensin HD5: crucial role for hydrophobicity at dimer interface. J
618 Biol Chem. 2012;287(26):21615-27. Epub 20120509. doi: 10.1074/jbc.M112.367995.
619 PubMed PMID: 22573326; PubMed Central PMCID: PMCPMC3381126.

620 21. Gounder AP, Wiens ME, Wilson SS, Lu W, Smith JG. Critical determinants of human alpha-
621 defensin 5 activity against non-enveloped viruses. J Biol Chem. 2012;287(29):24554-62.
622 Epub 20120525. doi: 10.1074/jbc.M112.354068. PubMed PMID: 22637473; PubMed
623 Central PMCID: PMCPMC3397880.
624 22. Porter JM, Oswald MS, Sharma A, Emmanuel S, Kansol A, Bennett A, et al. A Single
625 Surface-Exposed Amino Acid Determines Differential Neutralization of AAV1 and AAV6 by
626 Human Alpha-Defensins. J Virol. 2023;97(3):e0006023. Epub 20230314. doi:
627 10.1128/jvi.00060-23. PubMed PMID: 36916912; PubMed Central PMCID:
628 PMCPMC10062168.
629 23. Xu C, Wang A, Marin M, Honnen W, Ramasamy S, Porter E, et al. Human Defensins Inhibit
630 SARS-CoV-2 Infection by Blocking Viral Entry. Viruses. 2021;13(7). Epub 20210626. doi:
631 10.3390/v13071246. PubMed PMID: 34206990; PubMed Central PMCID:
632 PMCPMC8310277.
633 24. Holly MK, Smith JG. Paneth Cells during Viral Infection and Pathogenesis. Viruses.
634 2018;10(5). Epub 20180426. doi: 10.3390/v10050225. PubMed PMID: 29701691; PubMed
635 Central PMCID: PMCPMC5977218.
636 25. Spencer JD, Hains DS, Porter E, Bevins CL, DiRosario J, Becknell B, et al. Human alpha
637 defensin 5 expression in the human kidney and urinary tract. PLoS One. 2012;7(2):e31712.
638 Epub 20120216. doi: 10.1371/journal.pone.0031712. PubMed PMID: 22359618; PubMed
639 Central PMCID: PMCPMC3281003.
640 26. Wehkamp J, Chu H, Shen B, Feathers RW, Kays RJ, Lee SK, et al. Paneth cell antimicrobial
641 peptides: topographical distribution and quantification in human gastrointestinal tissues.
642 FEBS Lett. 2006;580(22):5344-50. Epub 2006/09/23. doi: 10.1016/j.febslet.2006.08.083.
643 PubMed PMID: 16989824.

644 27. Ayabe T, Satchell DP, Wilson CL, Parks WC, Selsted ME, Ouellette AJ. Secretion of
645 microbicidal alpha-defensins by intestinal Paneth cells in response to bacteria. Nat Immunol.
646 2000;1(2):113-8. Epub 2001/03/15. doi: 10.1038/77783. PubMed PMID: 11248802.
647 28. Brinkmann V, Reichard U, Goosmann C, Fauler B, Uhlemann Y, Weiss DS, et al. Neutrophil
648 extracellular traps kill bacteria. Science. 2004;303(5663):1532-5. doi:
649 10.1126/science.1092385. PubMed PMID: 15001782.
650 29. Melle C, Ernst G, Schimmel B, Bleul A, Thieme H, Kaufmann R, et al. Discovery and
651 identification of alpha-defensins as low abundant, tumor-derived serum markers in
652 colorectal cancer. Gastroenterology. 2005;129(1):66-73. doi: 10.1053/j.gastro.2005.05.014.
653 PubMed PMID: 16012935.
654 30. Müller CA, Markovic-Lipkovski J, Klatt T, Gamper J, Schwarz G, Beck H, et al. Human α-
655 defensins HNPs-1,-2, and-3 in renal cell carcinoma: Influences on tumor cell proliferation.
656 The American journal of pathology. 2002;160(4):1311-24.
657 31. Huang C, Lou C, Zheng X, Pang L, Wang G, Zhu M, et al. Plasma human neutrophil peptides
658 as biomarkers of disease severity and mortality in patients with decompensated cirrhosis.
659 Liver Int. 2023;43(5):1096-106. Epub 20230128. doi: 10.1111/liv.15520. PubMed PMID:
660 36648384.
661 32. Rycyk-Bojarzynska A, Kasztelan-Szczerbinska B, Cichoz-Lach H, Surdacka A, Rolinski J.
662 Human Neutrophil Alpha-Defensins Promote NETosis and Liver Injury in Alcohol-Related
663 Liver Cirrhosis: Potential Therapeutic Agents. J Clin Med. 2024;13(5). Epub 20240222. doi:
664 10.3390/jcm13051237. PubMed PMID: 38592082; PubMed Central PMCID:
665 PMCPMC10931661.
666 33. Xu D, Lu W. Defensins: A Double-Edged Sword in Host Immunity. Front Immunol.
667 2020;11:764. Epub 2020/05/28. doi: 10.3389/fimmu.2020.00764. PubMed PMID:
668 32457744; PubMed Central PMCID: PMCPMC7224315.

669 34. Panyutich AV, Panyutich EA, Krapivin VA, Baturevich EA, Ganz T. Plasma defensin
670 concentrations are elevated in patients with septicemia or bacterial meningitis. The Journal
671 of laboratory and clinical medicine. 1993;122(2):202-7. PubMed PMID: 8340706.
672 35. Hida RY, Ohashi Y, Takano Y, Dogru M, Goto E, Fujishima H, et al. Elevated levels of
673 human alpha -defensin in tears of patients with allergic conjunctival disease complicated by
674 corneal lesions: detection by SELDI ProteinChip system and quantification. Curr Eye Res.
675 2005;30(9):723-30. doi: 10.1080/02713680591005986. PubMed PMID: 16123017.
676 36. Gokcinar NB, Karabulut AA, Onaran Z, Yumusak E, Budak Yildiran FA. Elevated Tear
677 Human Neutrophil Peptides 1-3, Human Beta Defensin-2 Levels and Conjunctival
678 Cathelicidin LL-37 Gene Expression in Ocular Rosacea. Ocular immunology and
679 inflammation. 2019;27(7):1174-83. Epub 20180824. doi: 10.1080/09273948.2018.1504971.
680 PubMed PMID: 30142005.
681 37. Virella-Lowell I, Poirier A, Chesnut KA, Brantly M, Flotte TR. Inhibition of recombinant
682 adeno-associated virus (rAAV) transduction by bronchial secretions from cystic fibrosis
683 patients. Gene Ther. 2000;7(20):1783-9. doi: 10.1038/sj.gt.3301268. PubMed PMID:
684 11083501.
685 38. Smith JG, Nemerow GR. Mechanism of adenovirus neutralization by Human alpha-
686 defensins. Cell host & microbe. 2008;3(1):11-9. Epub 2008/01/15. doi:
687 10.1016/j.chom.2007.12.001. PubMed PMID: 18191790.
688 39. Smith JG, Silvestry M, Lindert S, Lu W, Nemerow GR, Stewart PL. Insight into the
689 mechanisms of adenovirus capsid disassembly from studies of defensin neutralization.
690 PLoS Pathog. 2010;6(6):e1000959. Epub 20100624. doi: 10.1371/journal.ppat.1000959.
691 PubMed PMID: 20585634; PubMed Central PMCID: PMCPMC2891831.
692 40. Wiens ME, Smith JG. Alpha-defensin HD5 inhibits furin cleavage of human papillomavirus
693 16 L2 to block infection. J Virol. 2015;89(5):2866-74. Epub 20141224. doi:

694 10.1128/JVI.02901-14. PubMed PMID: 25540379; PubMed Central PMCID:
695 PMCPMC4325740.
696 41. Wiens ME, Smith JG. alpha-Defensin HD5 Inhibits Human Papillomavirus 16 Infection via
697 Capsid Stabilization and Redirection to the Lysosome. mBio. 2017;8(1). Epub 20170124.
698 doi: 10.1128/mBio.02304-16. PubMed PMID: 28119475; PubMed Central PMCID:
699 PMCPMC5263252.
700 42. Buck CB, Day PM, Thompson CD, Lubkowski J, Lu W, Lowy DR, et al. Human alpha-
701 defensins block papillomavirus infection. Proc Natl Acad Sci U S A. 2006;103(5):1516-21.
702 Epub 20060123. doi: 10.1073/pnas.0508033103. PubMed PMID: 16432216; PubMed
703 Central PMCID: PMCPMC1360544.
704 43. Dugan AS, Maginnis MS, Jordan JA, Gasparovic ML, Manley K, Page R, et al. Human alpha-
705 defensins inhibit BK virus infection by aggregating virions and blocking binding to host cells.
706 J Biol Chem. 2008;283(45):31125-32. Epub 20080909. doi: 10.1074/jbc.M805902200.
707 PubMed PMID: 18782756; PubMed Central PMCID: PMCPMC2576552.
708 44. Zins SR, Nelson CD, Maginnis MS, Banerjee R, O'Hara BA, Atwood WJ. The human alpha
709 defensin HD5 neutralizes JC polyomavirus infection by reducing endoplasmic reticulum
710 traffic and stabilizing the viral capsid. J Virol. 2014;88(2):948-60. Epub 20131106. doi:
711 10.1128/JVI.02766-13. PubMed PMID: 24198413; PubMed Central PMCID:
712 PMCPMC3911681.
713 45. Hu CT, Diaz K, Yang LC, Sharma A, Greenberg HB, Smith JG. Corrected and republished
714 from: "VP4 Is a Determinant of Alpha-Defensin Modulation of Rotaviral Infection". J Virol.
715 2023;97(10):e0096223. Epub 20231003. doi: 10.1128/jvi.00962-23. PubMed PMID:
716 37787534; PubMed Central PMCID: PMCPMC10617384.
717 46. Diaz K, Hu CT, Sul Y, Bromme BA, Myers ND, Skorohodova KV, et al. Defensin-driven viral
718 evolution. PLoS Pathog. 2020;16(11):e1009018. Epub 20201124. doi:

719 10.1371/journal.ppat.1009018. PubMed PMID: 33232373; PubMed Central PMCID:
720 PMCPMC7723274.
721 47. Nguyen EK, Nemerow GR, Smith JG. Direct evidence from single-cell analysis that human
722 alpha-defensins block adenovirus uncoating to neutralize infection. J Virol.
723 2010;84(8):4041-9. Epub 20100203. doi: 10.1128/JVI.02471-09. PubMed PMID: 20130047;
724 PubMed Central PMCID: PMCPMC2849482.
725 48. Tenge VR, Gounder AP, Wiens ME, Lu W, Smith JG. Delineation of interfaces on human
726 alpha-defensins critical for human adenovirus and human papillomavirus inhibition. PLoS
727 Pathog. 2014;10(9):e1004360. Epub 20140904. doi: 10.1371/journal.ppat.1004360.
728 PubMed PMID: 25188351; PubMed Central PMCID: PMCPMC4154873.
729 49. Bartlett JS, Wilcher R, Samulski RJ. Infectious entry pathway of adeno-associated virus and
730 adeno-associated virus vectors. J Virol. 2000;74(6):2777-85. PubMed PMID: 10684294.
731 50. Girod A, Wobus CE, Zadori Z, Ried M, Leike K, Tijssen P, et al. The VP1 capsid protein of
732 adeno-associated virus type 2 is carrying a phospholipase A2 domain required for virus
733 infectivity. J Gen Virol. 2002;83(Pt 5):973-8. Epub 2002/04/19. doi: 10.1099/0022-1317-83-
734 5-973. PubMed PMID: 11961250.
735 51. Kronenberg S, Bottcher B, von der Lieth CW, Bleker S, Kleinschmidt JA. A conformational
736 change in the adeno-associated virus type 2 capsid leads to the exposure of hidden VP1 N
737 termini. J Virol. 2005;79(9):5296-303. Epub 2005/04/14. doi: 10.1128/JVI.79.9.5296-
738 5303.2005. PubMed PMID: 15827144; PubMed Central PMCID: PMCPMC1082756.
739 52. Sonntag F, Bleker S, Leuchs B, Fischer R, Kleinschmidt JA. Adeno-associated virus type 2
740 capsids with externalized VP1/VP2 trafficking domains are generated prior to passage
741 through the cytoplasm and are maintained until uncoating occurs in the nucleus. J Virol.
742 2006;80(22):11040-54. Epub 20060906. doi: 10.1128/JVI.01056-06. PubMed PMID:
743 16956943; PubMed Central PMCID: PMCPMC1642181.

744 53. Stahnke S, Lux K, Uhrig S, Kreppel F, Hosel M, Coutelle O, et al. Intrinsic phospholipase
745 A2 activity of adeno-associated virus is involved in endosomal escape of incoming particles.
746 Virology. 2011;409(1):77-83. Epub 20101025. doi: 10.1016/j.virol.2010.09.025. PubMed
747 PMID: 20974479.
748 54. Wobus CE, Hugle-Dorr B, Girod A, Petersen G, Hallek M, Kleinschmidt JA. Monoclonal
749 antibodies against the adeno-associated virus type 2 (AAV-2) capsid: epitope mapping and
750 identification of capsid domains involved in AAV-2-cell interaction and neutralization of AAV-
751 2 infection. J Virol. 2000;74(19):9281-93. Epub 2000/09/12. doi: 10.1128/jvi.74.19.9281-
752 9293.2000. PubMed PMID: 10982375; PubMed Central PMCID: PMCPMC102127.
753 55. Wistuba A, Kern A, Weger S, Grimm D, Kleinschmidt JA. Subcellular compartmentalization
754 of adeno-associated virus type 2 assembly. J Virol. 1997;71(2):1341-52. doi:
755 10.1128/JVI.71.2.1341-1352.1997. PubMed PMID: 8995658; PubMed Central PMCID:
756 PMCPMC191189.
757 56. Huang LY, Patel A, Ng R, Miller EB, Halder S, McKenna R, et al. Characterization of the
758 Adeno-Associated Virus 1 and 6 Sialic Acid Binding Site. J Virol. 2016;90(11):5219-30. Epub
759 20160512. doi: 10.1128/JVI.00161-16. PubMed PMID: 26962225; PubMed Central PMCID:
760 PMCPMC4934739.
761 57. Kuck D, Kern A, Kleinschmidt JA. Development of AAV serotype-specific ELISAs using
762 novel monoclonal antibodies. J Virol Methods. 2007;140(1-2):17-24. Epub 20061128. doi:
763 10.1016/j.jviromet.2006.10.005. PubMed PMID: 17126418.
764 58. Li W, Zhang L, Wu Z, Pickles RJ, Samulski RJ. AAV-6 mediated efficient transduction of
765 mouse lower airways. Virology. 2011;417(2):327-33. Epub 20110714. doi:
766 10.1016/j.virol.2011.06.009. PubMed PMID: 21752418; PubMed Central PMCID:
767 PMCPMC3163804.
768 59. Salganik M, Venkatakrishnan B, Bennett A, Lins B, Yarbrough J, Muzyczka N, et al.
769 Evidence for pH-dependent protease activity in the adeno-associated virus capsid. J Virol.

770 2012;86(21):11877-85. Epub 20120822. doi: 10.1128/JVI.01717-12. PubMed PMID:
771 22915820; PubMed Central PMCID: PMCPMC3486322.
772 60. Rayaprolu V, Kruse S, Kant R, Venkatakrishnan B, Movahed N, Brooke D, et al.
773 Comparative analysis of adeno-associated virus capsid stability and dynamics. J Virol.
774 2013;87(24):13150-60. Epub 2013/09/27. doi: 10.1128/JVI.01415-13. PubMed PMID:
775 24067976; PubMed Central PMCID: PMCPMC3838259.
776 61. Lins-Austin B, Patel S, Mietzsch M, Brooke D, Bennett A, Venkatakrishnan B, et al. Adeno-
777 Associated Virus (AAV) Capsid Stability and Liposome Remodeling During Endo/Lysosomal
778 pH Trafficking. Viruses. 2020;12(6). Epub 2020/06/25. doi: 10.3390/v12060668. PubMed
779 PMID: 32575696; PubMed Central PMCID: PMCPMC7354436.
780 62. Grieger JC, Snowdy S, Samulski RJ. Separate basic region motifs within the adeno-
781 associated virus capsid proteins are essential for infectivity and assembly. J Virol.
782 2006;80(11):5199-210. Epub 2006/05/16. doi: 10.1128/JVI.02723-05. PubMed PMID:
783 16699000; PubMed Central PMCID: PMCPMC1472161.
784 63. Summerford C, Samulski RJ. Membrane-associated heparan sulfate proteoglycan is a
785 receptor for adeno-associated virus type 2 virions. J Virol. 1998;72(2):1438-45. Epub
786 1998/01/28. PubMed PMID: 9445046; PubMed Central PMCID: PMCPMC124624.
787 64. Wu Z, Asokan A, Grieger JC, Govindasamy L, Agbandje-McKenna M, Samulski RJ. Single
788 amino acid changes can influence titer, heparin binding, and tissue tropism in different
789 adeno-associated virus serotypes. J Virol. 2006;80(22):11393-7. Epub 20060830. doi:
790 10.1128/JVI.01288-06. PubMed PMID: 16943302; PubMed Central PMCID:
791 PMCPMC1642158.
792 65. Wu Z, Miller E, Agbandje-McKenna M, Samulski RJ. Alpha2,3 and alpha2,6 N-linked sialic
793 acids facilitate efficient binding and transduction by adeno-associated virus types 1 and 6.
794 J Virol. 2006;80(18):9093-103. Epub 2006/08/31. doi: 10.1128/JVI.00895-06. PubMed
795 PMID: 16940521; PubMed Central PMCID: PMCPMC1563919.

796 66. Zengel J, Carette JE. Structural and cellular biology of adeno-associated virus attachment
797 and entry. Adv Virus Res. 2020;106:39-84. Epub 20200213. doi:
798 10.1016/bs.aivir.2020.01.002. PubMed PMID: 32327148.
799 67. Dudek AM, Pillay S, Puschnik AS, Nagamine CM, Cheng F, Qiu J, et al. An Alternate Route
800 for Adeno-associated Virus (AAV) Entry Independent of AAV Receptor. J Virol. 2018;92(7).
801 Epub 2018/01/19. doi: 10.1128/JVI.02213-17. PubMed PMID: 29343568; PubMed Central
802 PMCID: PMCPMC5972900.
803 68. Pillay S, Meyer NL, Puschnik AS, Davulcu O, Diep J, Ishikawa Y, et al. An essential receptor
804 for adeno-associated virus infection. Nature. 2016;530(7588):108-12. Epub 20160127. doi:
805 10.1038/nature16465. PubMed PMID: 26814968; PubMed Central PMCID:
806 PMCPMC4962915.
807 69. Dudek AM, Zabaleta N, Zinn E, Pillay S, Zengel J, Porter C, et al. GPR108 Is a Highly
808 Conserved AAV Entry Factor. Mol Ther. 2020;28(2):367-81. Epub 20191113. doi:
809 10.1016/j.ymthe.2019.11.005. PubMed PMID: 31784416; PubMed Central PMCID:
810 PMCPMC7000996.
811 70. Meisen WH, Nejad ZB, Hardy M, Zhao H, Oliverio O, Wang S, et al. Pooled Screens Identify
812 GPR108 and TM9SF2 as Host Cell Factors Critical for AAV Transduction. Mol Ther Methods
813 Clin Dev. 2020;17:601-11. Epub 20200317. doi: 10.1016/j.omtm.2020.03.012. PubMed
814 PMID: 32280726; PubMed Central PMCID: PMCPMC7139131.
815 71. Mantyla E, Kann M, Vihinen-Ranta M. Protoparvovirus Knocking at the Nuclear Door.
816 Viruses. 2017;9(10). Epub 20171002. doi: 10.3390/v9100286. PubMed PMID: 28974036;
817 PubMed Central PMCID: PMCPMC5691637.
818 72. Sanlioglu S, Benson PK, Yang J, Atkinson EM, Reynolds T, Engelhardt JF. Endocytosis and
819 nuclear trafficking of adeno-associated virus type 2 are controlled by rac1 and
820 phosphatidylinositol-3 kinase activation. J Virol. 2000;74(19):9184-96. doi:

821 10.1128/jvi.74.19.9184-9196.2000. PubMed PMID: 10982365; PubMed Central PMCID:
822 PMCPMC102117.
823 73. Xiao PJ, Samulski RJ. Cytoplasmic trafficking, endosomal escape, and perinuclear
824 accumulation of adeno-associated virus type 2 particles are facilitated by microtubule
825 network. J Virol. 2012;86(19):10462-73. Epub 20120718. doi: 10.1128/JVI.00935-12.
826 PubMed PMID: 22811523; PubMed Central PMCID: PMCPMC3457265.
827 74. Sutter SO, Lkharrazi A, Schraner EM, Michaelsen K, Meier AF, Marx J, et al. Adeno-
828 associated virus type 2 (AAV2) uncoating is a stepwise process and is linked to structural
829 reorganization of the nucleolus. PLoS Pathog. 2022;18(7):e1010187. Epub 20220711. doi:
830 10.1371/journal.ppat.1010187. PubMed PMID: 35816507; PubMed Central PMCID:
831 PMCPMC9302821.
832 75. Johnson JS, Samulski RJ. Enhancement of adeno-associated virus infection by mobilizing
833 capsids into and out of the nucleolus. J Virol. 2009;83(6):2632-44. Epub 20081224. doi:
834 10.1128/JVI.02309-08. PubMed PMID: 19109385; PubMed Central PMCID:
835 PMCPMC2648275.
836 76. Venkatakrishnan B, Yarbrough J, Domsic J, Bennett A, Bothner B, Kozyreva OG, et al.
837 Structure and dynamics of adeno-associated virus serotype 1 VP1-unique N-terminal
838 domain and its role in capsid trafficking. J Virol. 2013;87(9):4974-84. Epub 20130220. doi:
839 10.1128/JVI.02524-12. PubMed PMID: 23427155; PubMed Central PMCID:
840 PMCPMC3624325.
841 77. Bleker S, Sonntag F, Kleinschmidt JA. Mutational analysis of narrow pores at the fivefold
842 symmetry axes of adeno-associated virus type 2 capsids reveals a dual role in genome
843 packaging and activation of phospholipase A2 activity. J Virol. 2005;79(4):2528-40. doi:
844 10.1128/JVI.79.4.2528-2540.2005. PubMed PMID: 15681453; PubMed Central PMCID:
845 PMCPMC546590.

846 78. Horowitz ED, Finn MG, Asokan A. Tyrosine cross-linking reveals interfacial dynamics in
847 adeno-associated viral capsids during infection. ACS Chem Biol. 2012;7(6):1059-66. Epub
848 20120406. doi: 10.1021/cb3000265. PubMed PMID: 22458529; PubMed Central PMCID:
849 PMCPMC3376196.
850 79. Emmanuel SN, Smith JK, Hsi J, Tseng YS, Kaplan M, Mietzsch M, et al. Structurally
851 Mapping Antigenic Epitopes of Adeno-associated Virus 9: Development of Antibody Escape
852 Variants. J Virol. 2022;96(3):e0125121. Epub 20211110. doi: 10.1128/JVI.01251-21.
853 PubMed PMID: 34757842; PubMed Central PMCID: PMCPMC8827038.
854 80. Havlik LP, Simon KE, Smith JK, Klinc KA, Tse LV, Oh DK, et al. Coevolution of Adeno-
855 associated Virus Capsid Antigenicity and Tropism through a Structure-Guided Approach. J
856 Virol. 2020;94(19). Epub 20200915. doi: 10.1128/JVI.00976-20. PubMed PMID: 32669336;
857 PubMed Central PMCID: PMCPMC7495376.
858 81. Mietzsch M, Smith JK, Yu JC, Banala V, Emmanuel SN, Jose A, et al. Characterization of
859 AAV-Specific Affinity Ligands: Consequences for Vector Purification and Development
860 Strategies. Mol Ther Methods Clin Dev. 2020;19:362-73. Epub 20201004. doi:
861 10.1016/j.omtm.2020.10.001. PubMed PMID: 33145372; PubMed Central PMCID:
862 PMCPMC7591348.
863 82. Kurian JJ, Lakshmanan R, Chmely WM, Hull JA, Yu JC, Bennett A, et al. Adeno-Associated
864 Virus VP1u Exhibits Protease Activity. Viruses. 2019;11(5). Epub 20190429. doi:
865 10.3390/v11050399. PubMed PMID: 31035643; PubMed Central PMCID:
866 PMCPMC6563295.
867 83. Farr GA, Cotmore SF, Tattersall P. VP2 cleavage and the leucine ring at the base of the
868 fivefold cylinder control pH-dependent externalization of both the VP1 N terminus and the
869 genome of minute virus of mice. J Virol. 2006;80(1):161-71. doi: 10.1128/JVI.80.1.161-
870 171.2006. PubMed PMID: 16352540; PubMed Central PMCID: PMCPMC1317546.

871 84. Callaway HM, Feng KH, Lee DW, Allison AB, Pinard M, McKenna R, et al. Parvovirus Capsid
872 Structures Required for Infection: Mutations Controlling Receptor Recognition and Protease
873 Cleavages. J Virol. 2017;91(2). Epub 20170103. doi: 10.1128/JVI.01871-16. PubMed PMID:
874 27847360; PubMed Central PMCID: PMCPMC5215354.
875 85. Mani B, Baltzer C, Valle N, Almendral JM, Kempf C, Ros C. Low pH-dependent endosomal
876 processing of the incoming parvovirus minute virus of mice virion leads to externalization of
877 the VP1 N-terminal sequence (N-VP1), N-VP2 cleavage, and uncoating of the full-length
878 genome. J Virol. 2006;80(2):1015-24. doi: 10.1128/JVI.80.2.1015-1024.2006. PubMed
879 PMID: 16379002; PubMed Central PMCID: PMCPMC1346861.
880 86. Zhao C, Porter JM, Burke PC, Arnberg N, Smith JG. Alpha-defensin binding expands human
881 adenovirus tropism. PLoS Pathog. 2024;20(6):e1012317. Epub 20240620. doi:
882 10.1371/journal.ppat.1012317. PubMed PMID: 38900833; PubMed Central PMCID:
883 PMCPMC11230588.
884 87. Wilson SS, Bromme BA, Holly MK, Wiens ME, Gounder AP, Sul Y, et al. Alpha-defensin-
885 dependent enhancement of enteric viral infection. PLoS Pathog. 2017;13(6):e1006446.
886 Epub 20170616. doi: 10.1371/journal.ppat.1006446. PubMed PMID: 28622386; PubMed
887 Central PMCID: PMCPMC5489213.
888 88. Rapista A, Ding J, Benito B, Lo YT, Neiditch MB, Lu W, et al. Human defensins 5 and 6
889 enhance HIV-1 infectivity through promoting HIV attachment. Retrovirology. 2011;8:45.
890 Epub 20110614. doi: 10.1186/1742-4690-8-45. PubMed PMID: 21672195; PubMed Central
891 PMCID: PMCPMC3146398.
892 89. Hazlett L, Wu M. Defensins in innate immunity. Cell Tissue Res. 2011;343(1):175-88. Epub
893 20100821. doi: 10.1007/s00441-010-1022-4. PubMed PMID: 20730446.
894 90. Yan Z, Zak R, Zhang Y, Ding W, Godwin S, Munson K, et al. Distinct classes of proteasome-
895 modulating agents cooperatively augment recombinant adeno-associated virus type 2 and
896 type 5-mediated transduction from the apical surfaces of human airway epithelia. J Virol.

897 2004;78(6):2863-74. doi: 10.1128/jvi.78.6.2863-2874.2004. PubMed PMID: 14990705;
898 PubMed Central PMCID: PMCPMC353734.
899 91. Rabinowitz JE, Rolling F, Li C, Conrath H, Xiao W, Xiao X, et al. Cross-packaging of a single
900 adeno-associated virus (AAV) type 2 vector genome into multiple AAV serotypes enables
901 transduction with broad specificity. J Virol. 2002;76(2):791-801. doi: 10.1128/jvi.76.2.791-
902 801.2002. PubMed PMID: 11752169; PubMed Central PMCID: PMCPMC136844.
903 92. Burger C, Gorbatyuk OS, Velardo MJ, Peden CS, Williams P, Zolotukhin S, et al.
904 Recombinant AAV viral vectors pseudotyped with viral capsids from serotypes 1, 2, and 5
905 display differential efficiency and cell tropism after delivery to different regions of the central
906 nervous system. Mol Ther. 2004;10(2):302-17. doi: 10.1016/j.ymthe.2004.05.024. PubMed
907 PMID: 15294177.
908 93. Xiao X, Li J, Samulski RJ. Production of high-titer recombinant adeno-associated virus
909 vectors in the absence of helper adenovirus. J Virol. 1998;72(3):2224-32. doi:
910 10.1128/JVI.72.3.2224-2232.1998. PubMed PMID: 9499080; PubMed Central PMCID:
911 PMCPMC109519.
912 94. Bennett A, Patel S, Mietzsch M, Jose A, Lins-Austin B, Yu JC, et al. Thermal Stability as a
913 Determinant of AAV Serotype Identity. Mol Ther Methods Clin Dev. 2017;6:171-82. Epub
914 20170724. doi: 10.1016/j.omtm.2017.07.003. PubMed PMID: 28828392; PubMed Central
915 PMCID: PMCPMC5552060.
916 95. Tseng YS, Gurda BL, Chipman P, McKenna R, Afione S, Chiorini JA, et al. Adeno-
917 associated virus serotype 1 (AAV1)- and AAV5-antibody complex structures reveal
918 evolutionary commonalities in parvovirus antigenic reactivity. J Virol. 2015;89(3):1794-808.
919 Epub 20141119. doi: 10.1128/JVI.02710-14. PubMed PMID: 25410874; PubMed Central
920 PMCID: PMCPMC4300747.

921 96. Pachitariu M, Stringer C. Cellpose 2.0: how to train your own model. Nat Methods.
922 2022;19(12):1634-41. Epub 20221107. doi: 10.1038/s41592-022-01663-4. PubMed PMID:
923 36344832; PubMed Central PMCID: PMCPMC9718665.
924 97. Stirling DR, Swain-Bowden MJ, Lucas AM, Carpenter AE, Cimini BA, Goodman A.
925 CellProfiler 4: improvements in speed, utility and usability. BMC Bioinformatics.
926 2021;22(1):433. Epub 20210910. doi: 10.1186/s12859-021-04344-9. PubMed PMID:
927 34507520; PubMed Central PMCID: PMCPMC8431850.

928

929 **Figure Legends**

930 **Figure 1. Both HD5 and HNP1 bind to AAV2 and neutralize infection.** Infection of AAV2 in the
931 presence of (A) HD5 or (B) HNP1. AAV2 was exposed to each defensin on ice prior to and during
932 HeLa cell infection. Data are normalized to control infection in the absence of defensin and are
933 the mean ± SD of a minimum of 3 independent experiments. Mean IC_{50} values are indicated. Both
934 (C) HD5 and (D) HNP1 bind to AAV2. Background-corrected SPR sensorgrams are shown from
935 a concentration series of defensin interacting with immobilized AAV2. Colors correspond to
936 analyte (defensin) concentration, as indicated. Sensorgrams are representative of 2 independent
937 replicates for each defensin. Mean K_D values ± SD are indicated.

938 **Figure 2. HD5, but not HNP1, inhibits AAV2 binding to cells, while both defensins impose**
939 **a post-attachment block to infection.** Effects of (A) HD5 and (B) HNP1 on AAV2 binding to
940 HeLa cells. AAV2 was exposed to each defensin on ice prior to and during HeLa cell binding,
941 which was then quantified by qPCR. Data are normalized to the amount of virus bound in the
942 absence of defensin and are the mean ± SD of at least 3 independent experiments. The mean
943 HD5 IC_{50} value is indicated. Both (C) HD5 and (D) HNP1 inhibit AAV2 infection when added after
944 attachment of AAV2 to cells. Data are normalized to control infection in the absence of defensin
945 and are the mean ± SD of a minimum of 3 independent experiments. Mean IC_{50} values are
946 indicated.

947 **Figure 3. Both HD5 and HNP1 block AAV2 VP1u exposure.** (A) Representative western blots
948 of AAV2 that was sequentially immunoprecipitated at 6 h p.i. first with the A1 (VP1u-specific)
949 antibody (top) then the A20 (intact capsid) antibody (bottom). Cells were infected in the presence
950 of 25 μM HD5, 25 μM HD5abu (ABU), or no defensin (ND). Uninfected cells (no virus, NV) were
951 included as a control. Blots were probed with the B1 antibody, and (B) the ratio of VP3 in the two
952 blots was quantified. Positions of VP1, VP2, and VP3 for all blots are labeled in panel G. (C)
953 Representative western blots and (D) quantification of similar experiments using 30 μM HNP1.

954 (E) Representative western blots and (F) quantification of control experiments where no defensin
955 was present at the time of infection, but 25 μM HD5 or no defensin (ND) was added to the cell
956 lysate prior to immunoprecipitation. (G) Representative western blots and (H) quantification of
957 similar experiments using 30 μM HNP1 post-lysis. (I and J) Representative images and (K)
958 quantification of HeLa cells in 96-well plates infected with AAV2 in the presence or absence of
959 the same concentrations of defensins that were used for immunoprecipitation. Images were
960 obtained 48 h p.i. at a resolution of 50 μm, and grayscale intensity correlates with eGFP
961 expression. Note that the infections were performed in parallel with the immunoprecipitation
962 experiments but that the HNP1 infection experiments were done separately from those with HD5
963 and HD5abu. For B, D, F, H, and I, each point is a biological replicate (n = 3), and bars are the
964 mean ± SD. Experiments in E and F used three times the culture size of the other panels, and
965 infections were stopped 5 h p.i. instead of 6 h p.i.

966 **Figure 4. HD5, but not HNP1, inhibits AAV6 binding to cells, while both defensins block**
967 **AAV6 VP1u exposure.** Effects of (A) HD5 and (B) HNP1 on AAV6 binding to HeLa cells. AAV6
968 was exposed to each defensin on ice prior to and during HeLa cell binding, which was then
969 quantified by qPCR. Data are normalized to the amount of virus bound in the absence of defensin
970 and are the mean ± SD of at least 3 independent experiments. The effects of HD5 and HNP1 on
971 AAV6 infection is reproduced from [22] for comparison. Data are normalized to control infection
972 in the absence of defensin and are the mean ± SD of a minimum of 3 independent experiments.
973 Mean IC_{50} values are indicated. (C) The neutralizing antibody ADK1a (1 μg/mL) and the lectin
974 wheat germ agglutinin (WGA, 50 μg/mL) both block AAV6 binding to HeLa cells. (D)
975 Representative western blots of AAV6 that was sequentially immunoprecipitated at 5 h p.i. first
976 with the A1 (VP1u-specific) antibody (top) then the ADK1a (intact capsid) antibody (bottom). Cells
977 were infected in the presence of 25 μM HD5, 30 μM HNP1, or no defensin (ND). Uninfected cells
978 (no virus, NV) were included as a control. Blots were probed with the B1 antibody, and (F) the

979 ratio of VP3 in the two blots was quantified then normalized to the ND control. (E) Representative
980 images and (G) quantification of HeLa cells in 96-well plates infected with AAV6 in the presence
981 or absence of the same concentrations of defensins that were used for immunoprecipitation.
982 Images were obtained 48 h p.i. at a resolution of 50 μm, and grayscale intensity correlates with
983 eGFP expression. For C, F, and G, each point is a biological replicate (n ≥ 3), and bars are the
984 mean ± SD.

985 **Figure 5. HD5 and HNP1 block proteolytic cleavage of the AAV2 capsid but do not alter**
986 **capsid thermostability.** Representative blots from additional replicates of the A20
987 immunoprecipitation experiments from Fig 3A and 3C probed with the B1 antibody. Arrows mark
988 a B1-reactive proteolytic fragment of the capsid proteins that is detectable in (A) the presence of
989 25 μM HD5abu (ABU) but not 25 μM HD5 and (B) the absence (ND) but not presence of 30 μM
990 HNP1. Uninfected cells (no virus, NV) were included as a control. (C) The melting temperature
991 (T_m) of AAV2 in the presence or absence of 25 μM HD5, 30 μM HNP1, or no defensin at the
992 indicated pHs. Each point is a biological replicate (n = 3), and bars are the mean ± SD.

993 **Figure 6. Both HD5 and HNP1 inhibit AAV2 nuclear localization.** (A-C) The fraction of DyLight
994 488 (DL488)-labelled AAV2 in the nucleus of HeLa cells infected in the presence of 25 μM HD5
995 or 30 μM HNP1 was assessed 24 h p.i. by confocal microscopy and automated image analysis.
996 Control cells infected in the absence of defensin (ND) were analyzed immediately after cold
997 synchronization (0 h p.i.) or at 24 h p.i. (A) Scatter plots with a minimum of 35 cells per condition
998 are shown. Each replicate is shown separately and indicated by both symbol (Replicate 1 =
999 circles, 2 = squares, 3 = triangles, 4 = upside-down triangles) and color shade. n.d. = not done.
1000 (B) Replicates from A were pooled and re-analyzed in aggregate for each condition. C)
1001 Representative images of single cells from the experiments in A. Merged images include DAPI
1002 (blue) and AAV2-DL488 (green). The fraction of DL488 signal in the nucleus is indicated for each
1003 merged image. (D) Representative images of single cells from the experiments in A are shown to

1004 depict the perinuclear region, located between the concentric yellow rings, which was used for
1005 the analysis in E. The fraction of DL488 signal in the nucleus (n) and perinuclear region (p) is
1006 indicated for each image. (E) The integrated intensity of the DL488 signal in the nucleus was
1007 divided by that of the perinuclear region, and the log of this ratio is graphed. (F) The total cellular
1008 integrated intensity of the DL488 signal was quantified. In all graphs, horizontal bars indicate
1009 means. In B, E, and F, the shape and color of each data point corresponds to the replicates and
1010 conditions in A. In C and D, scale bars indicate 10 μm, the DL488 signal was individually adjusted
1011 for display purposes, and cells are from different replicates across conditions.

1012 **Figure 7. Model of AAV neutralization by defensins.** Model of AAV infection in the absence
1013 (left) and presence (right) of neutralizing concentrations of HD5 or HNP1. Host factors including
1014 heparan sulfate proteoglycans (HSPG), the AAV receptor (AAVR), and GPR108 are depicted.
1015 The red “x” indicates the block to cell binding upon pre-attachment exposure of AAV2 or AAV6 to
1016 HD5. HNP1 is used to illustrate the effects of the intracellular defensin block, which is common to
1017 HD5 and HNP1. Figure created with BioRender.com.

1018

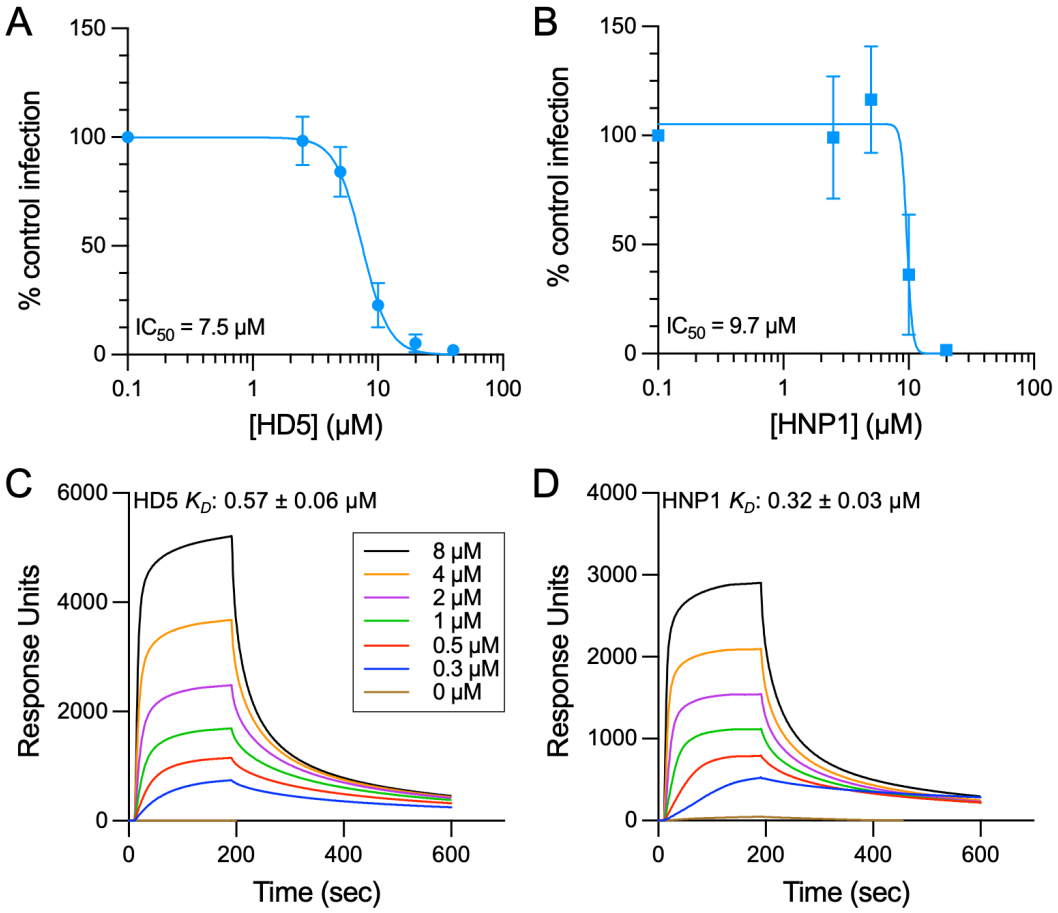

Figure 1. Both HD5 and HNP1 bind to AAV2 and neutralize infection. Infection of AAV2 in the presence of (A) HD5 or (B) HNP1. AAV2 was exposed to each defensin on ice prior to and during HeLa cell infection. Data are normalized to control infection in the absence of defensin and are the mean ± SD of a minimum of 3 independent experiments. Mean IC_{50} values are indicated. Both (C) HD5 and (D) HNP1 bind to AAV2. Background-corrected SPR sensorgrams are shown from a concentration series of defensin interacting with immobilized AAV2. Colors correspond to analyte (defensin) concentration, as indicated. Sensorgrams are representative of 2 independent replicates for each defensin. Mean K_D values ± SD are indicated.

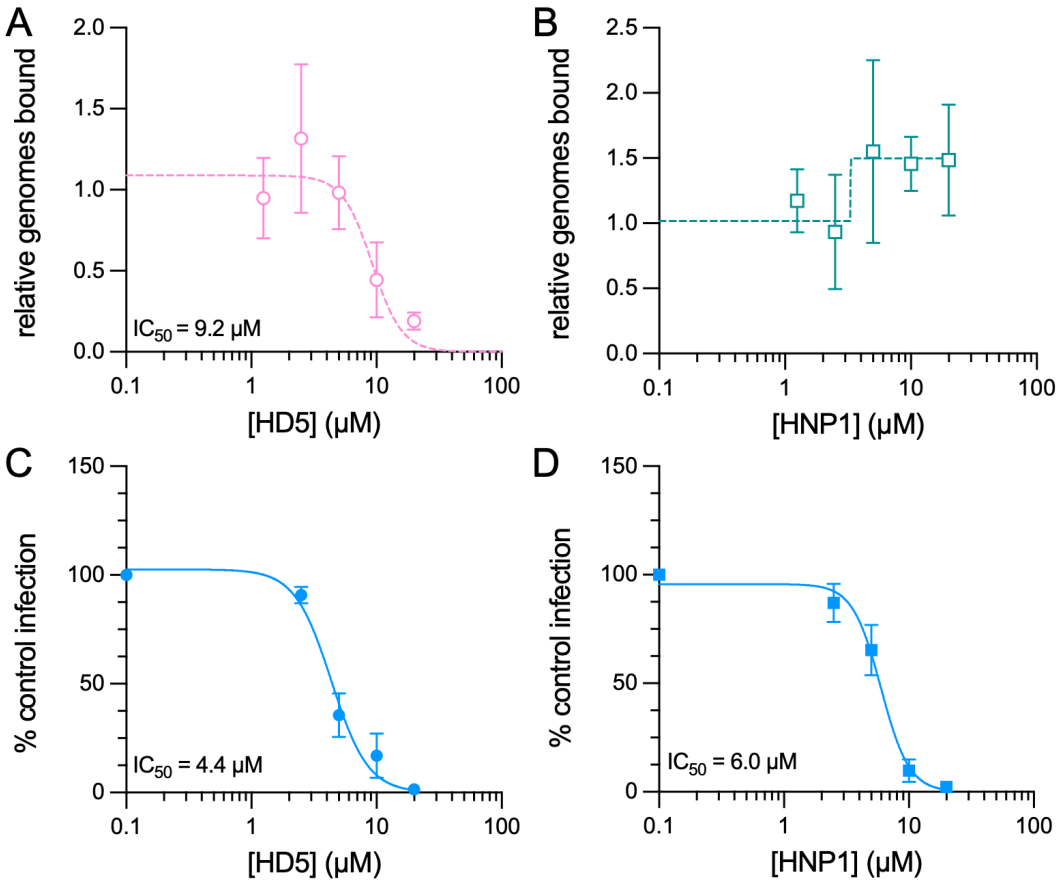

Figure 2. HD5, but not HNP1, inhibits AAV2 binding to cells, while both defensins impose a post-attachment block to infection. Effects of (A) HD5 and (B) HNP1 on AAV2 binding to HeLa cells. AAV2 was exposed to each defensin on ice prior to and during HeLa cell binding, which was then quantified by qPCR. Data are normalized to the amount of virus bound in the absence of defensin and are the mean ± SD of at least 3 independent experiments. The mean HD5 IC_{50} value is indicated. Both (C) HD5 and (D) HNP1 inhibit AAV2 infection when added after attachment of AAV2 to cells. Data are normalized to control infection in the absence of defensin and are the mean ± SD of a minimum of 3 independent experiments. Mean IC_{50} values are indicated.

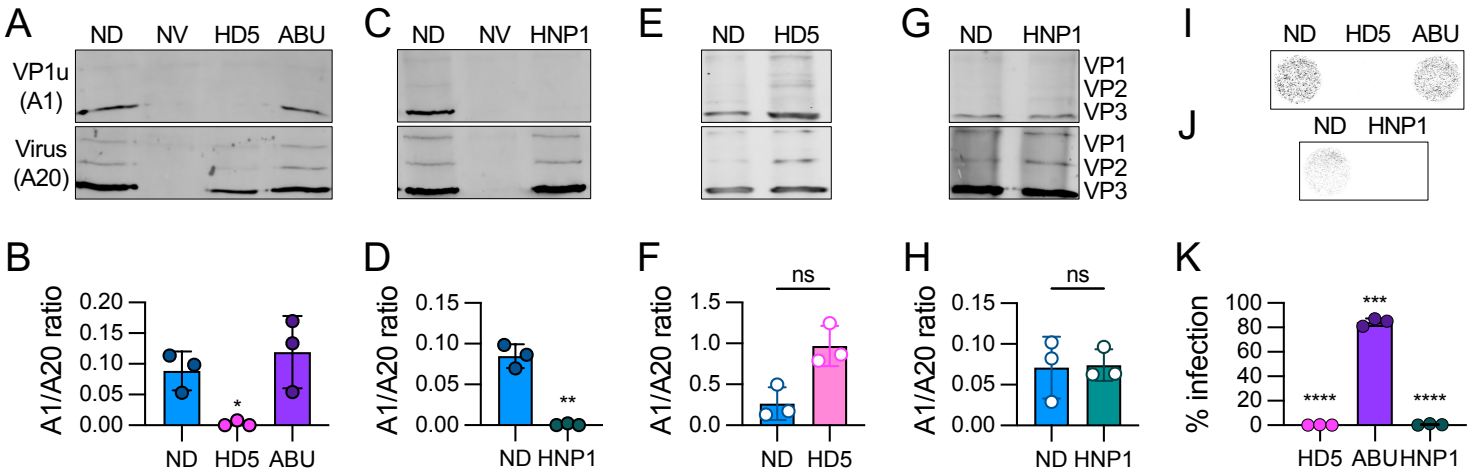

Figure 3. Both HD5 and HNP1 block AAV2 VP1u exposure. (A) Representative western blots of AAV2 that was sequentially immunoprecipitated at 6 h p.i. first with the A1 (VP1u-specific) antibody (top) then the A20 (intact capsid) antibody (bottom). Cells were infected in the presence of 25 μM HD5, 25 μM HD5abu (ABU), or no defensin (ND). Uninfected cells (no virus, NV) were included as a control. Blots were probed with the B1 antibody, and (B) the ratio of VP3 in the two blots was quantified. Positions of VP1, VP2, and VP3 for all blots are labeled in panel G. (C) Representative western blots and (D) quantification of similar experiments using 30 μM HNP1. (E) Representative western blots and (F) quantification of control experiments where no defensin was present at the time of infection, but 25 μM HD5 or no defensin (ND) was added to the cell lysate prior to immunoprecipitation. (G) Representative western blots and (H) quantification of similar experiments using 30 μM HNP1 post-lysis. (I and J) Representative images and (K) quantification of HeLa cells in 96-well plates infected with AAV2 in the presence or absence of the same concentrations of defensins that were used for immunoprecipitation. Images were obtained 48 h p.i. at a resolution of 50 μm, and grayscale intensity correlates with eGFP expression. Note that the infections were performed in parallel with the immunoprecipitation experiments but that the HNP1 infection experiments were done separately from those with HD5 and HD5abu. For B, D, F, H, and I, each point is a biological replicate (n = 3), and bars are the mean ± SD. Experiments in E and F used three times the culture size of the other panels, and infections were stopped 5 h p.i. instead of 6 h p.i.

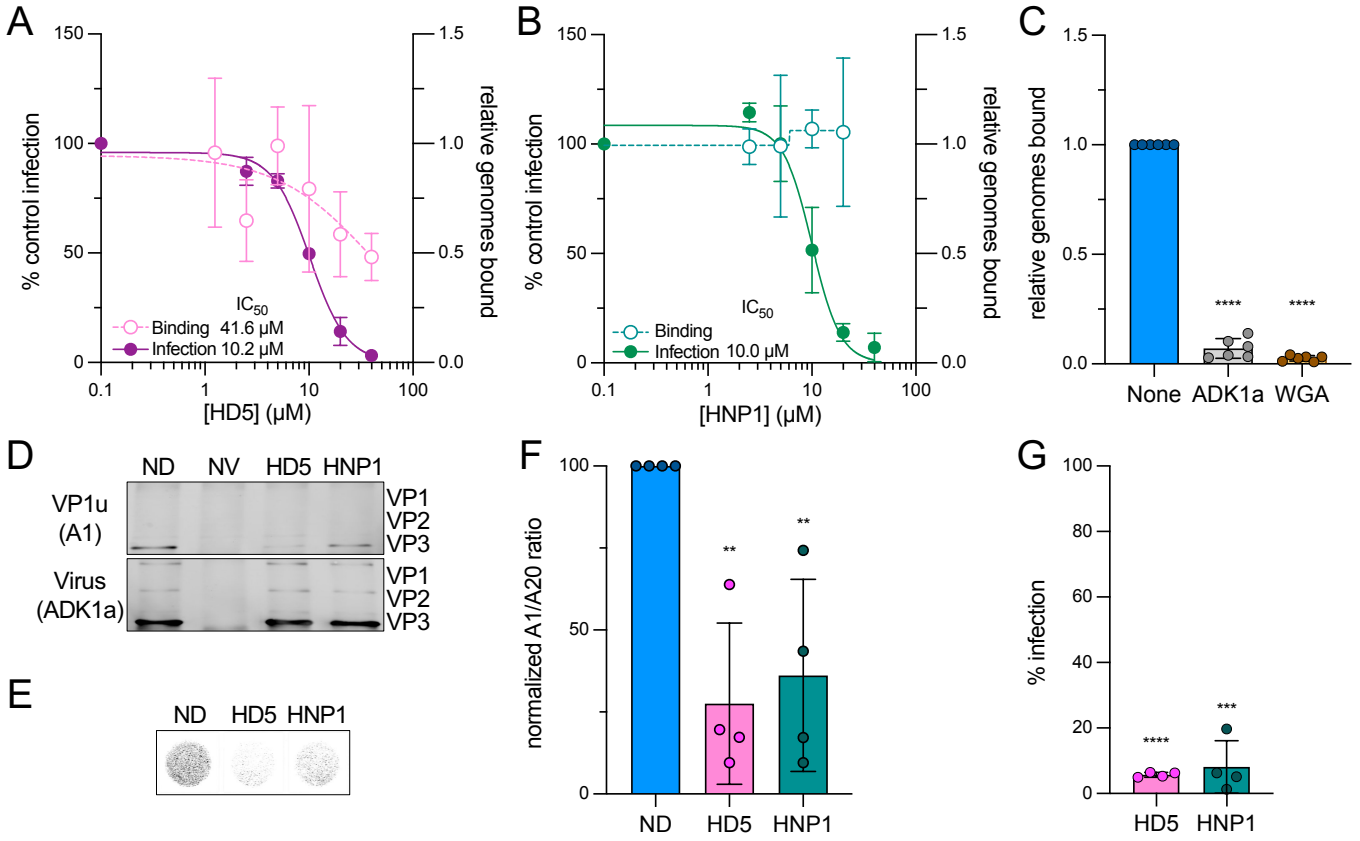

Figure 4. HD5, but not HNP1, inhibits AAV6 binding to cells, while both defensins block AAV6 VP1u exposure. Effects of (A) HD5 and (B) HNP1 on AAV6 binding to HeLa cells. AAV6 was exposed to each defensin on ice prior to and during HeLa cell binding, which was then quantified by qPCR. Data are normalized to the amount of virus bound in the absence of defensin and are the mean ± SD of at least 3 independent experiments. The effects of HD5 and HNP1 on AAV6 infection is reproduced from [22] for comparison. Data are normalized to control infection in the absence of defensin and are the mean ± SD of a minimum of 3 independent experiments. Mean IC50 values are indicated. (C) The neutralizing antibody ADK1a (1 μg/mL) and the lectin wheat germ agglutinin (WGA, 50 μg/mL) both block AAV6 binding to HeLa cells. (D) Representative western blots of AAV6 that was sequentially immunoprecipitated at 5 h p.i. first with the A1 (VP1u-specific) antibody (top) then the ADK1a (intact capsid) antibody (bottom). Cells were infected in the presence of 25 μM HD5, 30 μM HNP1, or no defensin (ND). Uninfected cells (no virus, NV) were included as a control. Blots were probed with the B1 antibody, and (F) the ratio of VP3 in the two blots was quantified then normalized to the ND control. (E) Representative images and (G) quantification of HeLa cells in 96-well plates infected with AAV6 in the presence or absence of the same concentrations of defensins that were used for immunoprecipitation. Images were obtained 48 h p.i. at a resolution of 50 μm, and grayscale intensity correlates with eGFP expression. For C, F, and G, each point is a biological replicate (n ≥ 3), and bars are the mean ± SD.

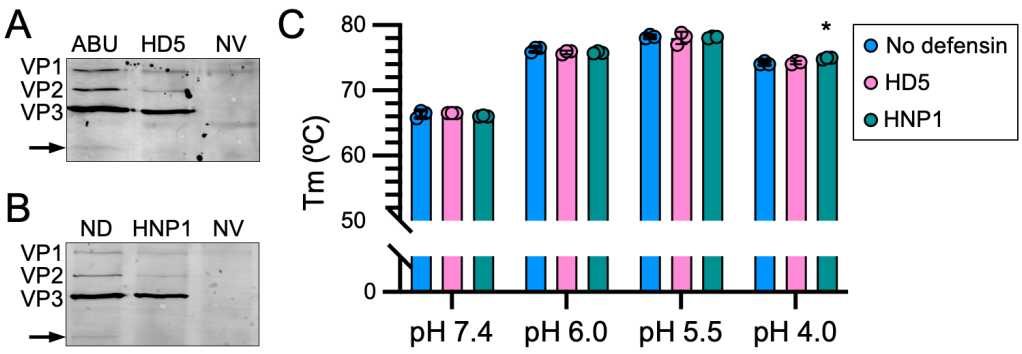

Figure 5. HD5 and HNP1 block proteolytic cleavage of the AAV2 capsid but do not alter capsid thermostability. Representative blots from additional replicates of the A20 immunoprecipitation experiments from Fig 3A and 3C probed with the B1 antibody. Arrows mark a B1-reactive proteolytic fragment of the capsid proteins that is detectable in (A) the presence of 25 μM HD5abu (ABU) but not 25 μM HD5 and (B) the absence (ND) but not presence of 30 μM HNP1. Uninfected cells (no virus, NV) were included as a control. (C) The melting temperature (T_m) of AAV2 in the presence or absence of 25 μM HD5, 30 μM HNP1, or no defensin at the indicated pHs. Each point is a biological replicate (n = 3), and bars are the mean ± SD.

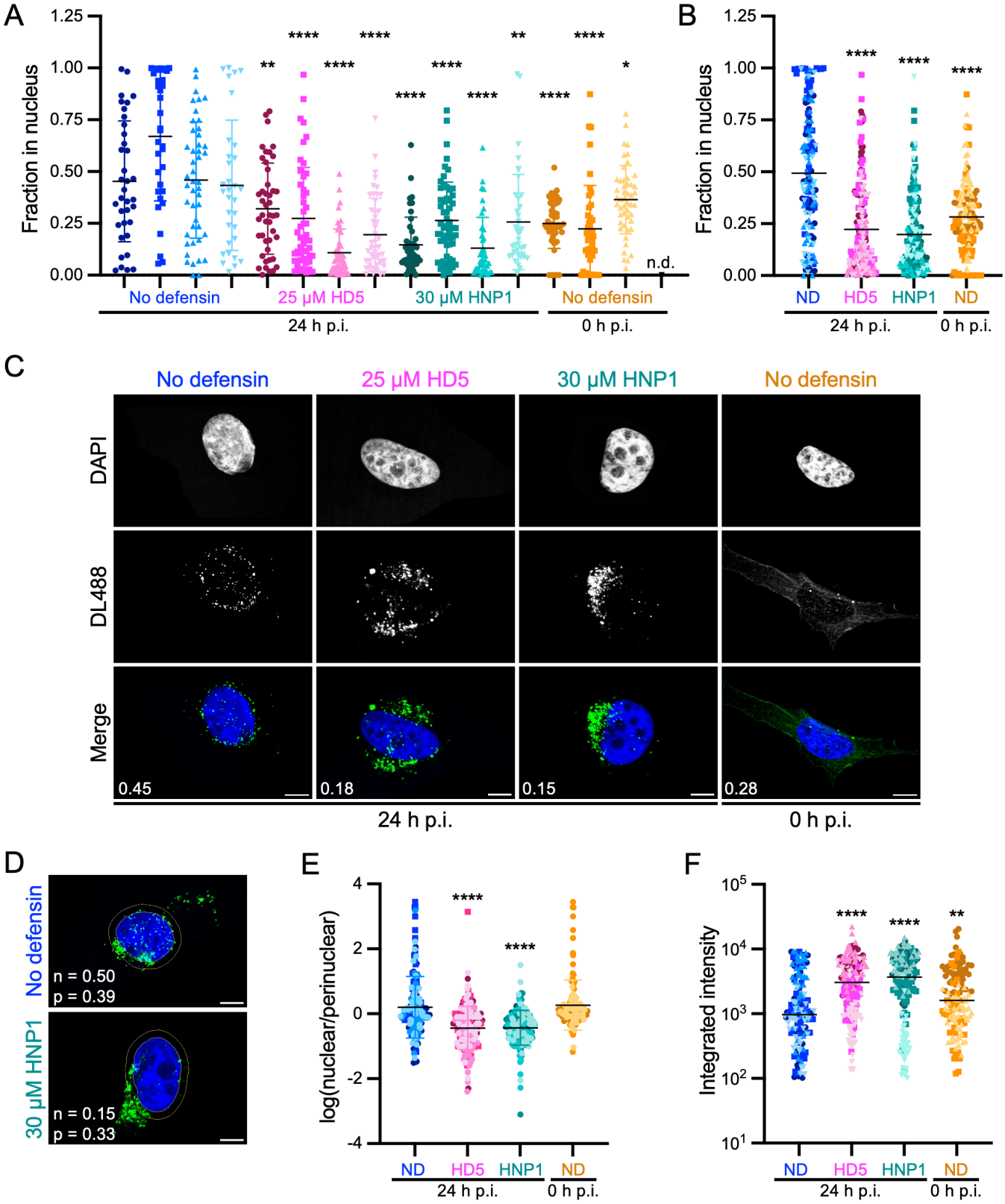
A
Fraction in nucleus
1.25
1.00
0.75
0.50
0.25
0.00
**
****
****
****
****
****
**
****
****
*
n.d.
No defensin
25 µM HD5
30 µM HNP1
No defensin
24 h p.i.
0 h p.i.
B
Fraction in nucleus
****
****
****
ND
HD5
HNP1
ND
24 h p.i.
0 h p.i.
C
No defensin
25 µM HD5
30 µM HNP1
No defensin
DAPI
DL488
Merge
0.45
0.18
0.15
0.28
24 h p.i.
0 h p.i.
D
No defensin
n = 0.50
p = 0.39
30 µM HNP1
n = 0.15
p = 0.33
E
log(nuclear/perinuclear)
4
2
0
-2
-4
****
****
ND
HD5
HNP1
ND
24 h p.i.
0 h p.i.
F
Integrated intensity
10^5
10^4
10^3
10^2
10^1
****
****
**
ND
HD5
HNP1
ND
24 h p.i.
0 h p.i.

Figure 6. Both HD5 and HNP1 inhibit AAV2 nuclear localization. (A-C) The fraction of DyLight 488 (DL488)-labelled AAV2 in the nucleus of HeLa cells infected in the presence of 25 μM HD5 or 30 μM HNP1 was assessed 24 h p.i. by confocal microscopy and automated image analysis. Control cells infected in the absence of defensin (ND) were analyzed immediately after cold synchronization (0 h p.i.) or at 24 h p.i. (A) Scatter plots with a minimum of 35 cells per condition are shown. Each replicate is shown separately and indicated by both symbol (Replicate 1 = circles, 2 = squares, 3 = triangles, 4 = upside-down triangles) and color shade. n.d. = not done. (B) Replicates from A were pooled and re-analyzed in aggregate for each condition. C) Representative images of single cells from the experiments in A. Merged images include DAPI (blue) and AAV2-DL488 (green). The fraction of DL488 signal in the nucleus is indicated for each merged image. (D) Representative images of single cells from the experiments in A are shown to depict the perinuclear region, located between the concentric yellow rings, which was used for the analysis in E. The fraction of DL488 signal in the nucleus (n) and perinuclear region (p) is indicated for each image. (E) The integrated intensity of the DL488 signal in the nucleus was divided by that of the perinuclear region, and the log of this ratio is graphed. (F) The total cellular integrated intensity of the DL488 signal was quantified. In all graphs, horizontal bars indicate means. In B, E, and F, the shape and color of each data point corresponds to the replicates and conditions in A. In C and D, scale bars indicate 10 μm, the DL488 signal was individually adjusted for display purposes, and cells are from different replicates across conditions.

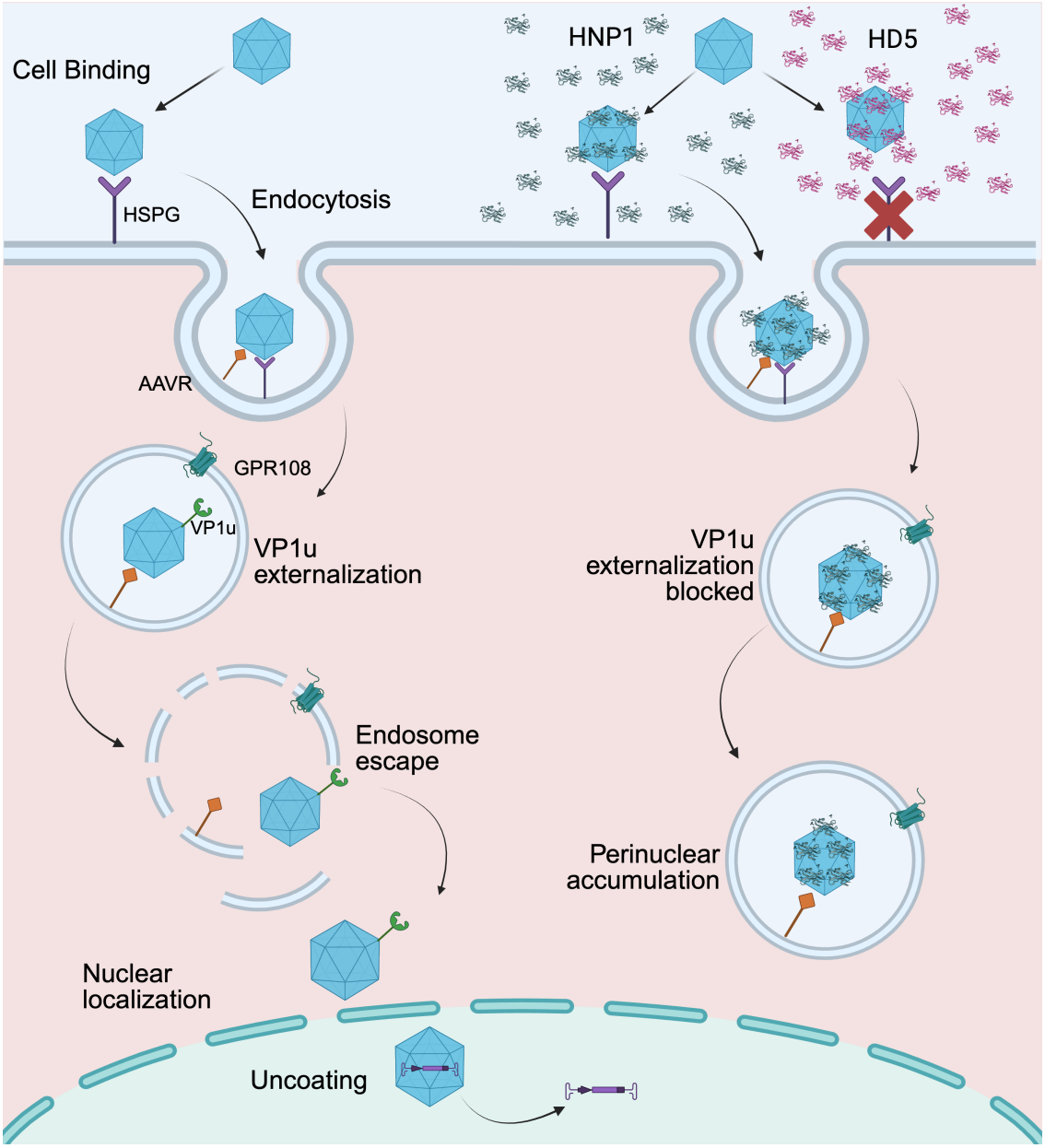

Figure 7. Model of AAV neutralization by defensins. Model of AAV infection in the absence (left) and presence (right) of neutralizing concentrations of HD5 or HNP1. Host factors including heparan sulfate proteoglycans (HSPG), the AAV receptor (AAVR), and GPR108 are depicted. The red "x" indicates the block to cell binding upon pre-attachment exposure of AAV2 or AAV6 to HD5. HNP1 is used to illustrate the effects of the intracellular defensin block, which is common to HD5 and HNP1. Figure created with BioRender.com.